

ENHANCEMENT OF PLASMONIC NONLINEAR CONVERSION AND
POLARIZATION LIFETIME VIA FANO RESONANCES

A THESIS SUBMITTED TO
THE GRADUATE SCHOOL OF NATURAL AND APPLIED SCIENCES
OF
MIDDLE EAST TECHNICAL UNIVERSITY

BY

BILGE CAN YILDIZ KARAKUL

IN PARTIAL FULFILLMENT OF THE REQUIREMENTS
FOR
THE DEGREE OF DOCTOR OF PHILOSOPHY
IN
PHYSICS

FEBRUARY 2017

Approval of the thesis:

**ENHANCEMENT OF PLASMONIC NONLINEAR CONVERSION AND
POLARIZATION LIFETIME VIA FANO RESONANCES**

submitted by **BILGE CAN YILDIZ KARAKUL** in partial fulfillment of the requirements for the degree of **Doctor of Philosophy in Physics Department, Middle East Technical University** by,

Prof. Dr. Gülbin Dural Ünver
Dean, Graduate School of **Natural and Applied Sciences**

Prof. Dr. Sadi Turgut
Head of Department, **Physics**

Assoc. Prof. Dr. Alpan Bek
Supervisor, **Department of Physics, METU**

Assoc. Prof. Dr. Mehmet Emre Taşgın
Co-supervisor, **Ins. of Nuclear Sciences, Hacettepe University**

Examining Committee Members:

Prof. Dr. Oğuz Gülseren
Department of Physics, Bilkent University

Assoc. Prof. Dr. Alpan Bek
Department of Physics, METU

Assoc. Prof. Dr. Ceyhun Bulutay
Department of Physics, Bilkent University

Assoc. Prof. Dr. Özgür Ergül
Department of Electrical and Electronics Engineering, METU

Assoc. Prof. Dr. Hande Toffoli
Department of Physics, METU

Date:

I hereby declare that all information in this document has been obtained and presented in accordance with academic rules and ethical conduct. I also declare that, as required by these rules and conduct, I have fully cited and referenced all material and results that are not original to this work.

Name, Last Name: BILGE CAN YILDIZ KARAKUL

Signature :

ABSTRACT

ENHANCEMENT OF PLASMONIC NONLINEAR CONVERSION AND POLARIZATION LIFETIME VIA FANO RESONANCES

Yıldız Karakul, Bilge Can

Ph.D., Department of Physics

Supervisor : Assoc. Prof. Dr. Alpan Bek

Co-Supervisor : Assoc. Prof. Dr. Mehmet Emre Taşgın

February 2017, 84 pages

Boundary conditions and dispersion at dielectric-conductor interfaces, together, results in bands of energies or wavelengths of light within which light-matter interaction strength displays peaks as a result of fulfilled resonance conditions. At these resonance energies light propagation is strongly coupled to collective oscillation of free charges at the dielectric-conductor interface which qualifies to be given a quasiparticle name, "the surface plasmon polariton" (SPP). When dealing with zero-dimensional metal nanostructures (MNSs) in dielectric environment, these SPPs are necessarily bound to the structure and cannot propagate, hence become localized surface plasmons (LSPs). Around resonant LSP wavelengths, light is effectively confined to nanoscale sizes in the near field of the supporting MNSs, which offers a playground for effective light-management at the nanoscale, hence applicability of concept of plasmonics arises in nanoscience and nanotechnology. Despite its high amplitude, induced polarization field at the MNS suffers from rapid decay in time due to Ohmic losses such as electron-core interactions. In this thesis, it is shown that when conditions are favorable, Fano resonances may offer lifetime enhancement in plasmonic oscillators as a result of coupling of short lifetime bright and long-lived dark plasmon oscillation modes. Fano resonance is a destructive path interference effect, which emerges as an asymmetric dip in the spectral response of a driven harmonic oscillator, when a short lifetime oscillator is driven by a harmonic field at the resonance

frequency of a long lifetime oscillator. At a certain frequency, the driven oscillator becomes under the influence of two driving forces which are out-of-phase, and hence their effects cancel each other. Time response of a plasmonic system can be extended by Fano resonance at a particular coupling strength, resonance and damping frequency. In addition, it is shown that Fano resonance mechanism is an effective way to enhance optical nonlinearities owing to plasmons in MNSs. Strong localized field leads to enhancement in higher harmonic fields compared to the linear responses. An analytical approach based on harmonic oscillator and a numerical approach based on 3D finite difference time domain Maxwell solution is presented to study the plasmonic coupling which resulted in prolonged lifetimes and enhanced or suppressed optical nonlinearity, in particular second harmonic generation. An experimental study on a silver coupled nanostructure system, results of which agree with the ones obtained in theory, is also presented as a verification of the developed model. Gaining the capability to obtain prolonged lifetime and enhanced nonlinear response of plasmonic MNS may play an important role for their successful integration to molecular switching, solar energy, photocatalysis and imaging applications.

Keywords: plasmon, nanoparticle, Fano resonance, lifetime, finite-difference time-domain, nonlinear conversion, second harmonic generation, enhancement

ÖZ

DOĞRUSAL OLMAYAN PLAZMONİK ÇEVİRİM VE POLARİZASYON YAŞAM SÜRESİNİN FANO REZONANSLAR İLE GÜÇENDİRİLMESİ

Yıldız Karakul, Bilge Can

Doktora, Fizik Bölümü

Tez Yöneticisi : Doç. Dr. Alpan Bek

Ortak Tez Yöneticisi : Doç. Dr. Mehmet Emre Taşgın

Şubat 2017 , 84 sayfa

Dielektrik-iletken arayüzlerdeki sınır koşulları ve dispersiyon, birlikte, içerisinde, ışık-madde etkileşim şiddetine göre, rezonans koşullarının sağlanmasının sonucu olarak pik noktaları elde edilen enerji veya dalgaboyu bantlarının oluşmasına yol açar. Bu rezonans enerjilerinde ışık yayılımı, dielektrik-iletken arayüzlerde meydana gelen ve yüzey plazmon polariton (YPP) adı verilerek nitelendirilen kuasi-parçacıklar ile, yani serbest yüklerin kolektif salınımı ile şiddetli bir şekilde çiftlenir. Söz konusu dielektrik ortamlardaki boyutsuz metal nanoyapılar (MNY) ise, bu YPPler yapıya bağlı olurlar ve yayılım yapamazlar, bu yüzden lokalize yüzey plazmonları (LYP) adı ile anılırlar. Rezonant LYP dalgaboyları civarında ışık, etkili bir şekilde MNYlerin yakın alanlarında, nano boyutlara hapsedilir. Bu durum nanoboyutta etkili bir ışık-manipülasyonu için ve bu yolla plazmonik kavramının nanobilim ve nanoteknoloji içerisinde uygulanabilirliğinin artması için zemin sağlar. Alan genliğinin çok güçlü olmasına rağmen, MNYler üzerinde indüklenmiş polarizasyon, elektron-çekirdek etkileşimi gibi Ohmik kayıplar nedeni ile çok hızlı bir şekilde sönümlenir. Bu tezde, elverişli koşullar altında Fano rezonansların, kısa yaşam süreli aydınlık modlar ile uzun yaşam süreli karanlık modlar arasındaki çiftlenmenin sonucu olarak, plazmonik salıngaçların yaşam sürelerini uzatabileceği gösterilmiştir. Fano rezonans, kısa yaşam süreli bir salıngacın, uzun yaşam süreli salıngacın rezonans frekansında bir harmonik alan ile sürülmesi ile meydana gelen ve sürülen salıngaçın spektral tepkisinde asimet-

rik bir dip olarak ortaya çıkan yıkıcı bir girişim yolu etkisidir. Belli bir frekansta sürülen salıngaç, efektif olarak, zıt fazlı olmaları sebebiyle birbirini sıfırlayan iki sürücü kuvvetin etkisi altında olur. Plazmonik bir sistemin zaman tepkisi, belli bir çiftlenme şiddeti, rezonans ve sönümlenme frekansında Fano rezonans ile uzatılabilir. Bununla beraber, Fano rezonans mekanizmasının, MNYler üzerindeki plazmonlar sayesinde optik doğrusalsızlığı güçlendirmenin etkili bir yolu olduğu gösterilmiştir. Güçlü bir şekilde lokalize edilmiş alan, doğrusal olana kıyasla yüksek harmonik alanların çok daha fazla güçlenmesine yol açar. Uzatılmış yaşam sürelerine ve güçlendirilmiş ya da baskılanmış ikinci harmonik çevirime sebep olan plazmonik çiftlenme kavramını çalışmak amacıyla, harmonik salıngaç yöntemine dayanan bir analitik yaklaşım ve zaman uzayında sonlu farklar yöntemi ile 3 boyutlu Maxwell çözümlerine dayanan bir sayısal yaklaşım sunulmuştur. Sonuçları, teorideki sonuçlar ile uyumlu olan, çiftlenmiş gümüş nanoyapılardan oluşan bir sistemin çalışıldığı bir deneysel çalışma da, geliştiren teorik modelin doğrulanması olarak sunulmuştur. Plazmonik MNYlerde uzatılmış yaşam süresi ve güçlendirilmiş doğrusal olmayan tepkinin elde edilmesi olanağını kazanmak, bunların, molekül anahtarlama, güneş enerjisi, fotokataliz ve görüntüleme gibi uygulamalara başarılı bir şekilde entegre edilebilmeleri açısından önemli bir rol oynayabilir.

Anahtar Kelimeler: plazmon, nanoparçacık, Fano rezonans, yaşam süresi, zaman-uzayında sonlu-farklar, doğrusal olmayan çevirim, ikinci harmonik çevirim, güçlendirme

To my beautiful daughter Deniz Can

ACKNOWLEDGMENTS

The author would like to express her gratitude and appreciation to her supervisor Dr. Alpan Bek for his guidance and encouragement, her cosupervisor Dr. Mehmet Emre Tasgin for his efforts in instructing on theoretical and computational work, and her colleague Musa Kurtuluş Abak for his suggestions especially in numerical simulations. TUBITAK grant nrs 113F239 and 115F603 are gratefully acknowledged.

TABLE OF CONTENTS

ABSTRACT	v
ÖZ	vii
ACKNOWLEDGMENTS	x
TABLE OF CONTENTS	xi
LIST OF TABLES	xiii
LIST OF FIGURES	xiv
LIST OF ABBREVIATIONS	xvi
CHAPTERS	
1 INTRODUCTION	1
2 THEORETICAL BACKGROUND	5
2.1 Plasmonic oscillations	5
2.1.1 Surface plasmon polaritons	6
2.1.2 Localized surface plasmons	7
2.2 Nonlinear plasmonics	8
2.2.1 Second harmonic generation	9
2.3 Fano resonance	10

3	LIFETIME ENHANCEMENT IN COUPLED PLASMONIC SYSTEMS	13
3.1	Eigenvalue problem of a coupled plasmonic system	14
3.1.1	Long term behaviour of the plasmon decay	20
3.1.2	Short term behaviour of the plasmon decay	30
3.2	Numerical Maxwell simulations for a 3D coupled plasmonic system	32
3.2.1	Short and long term behaviours of the energy	36
3.2.2	Hybridization in the scattering cross section	37
3.3	Summary and Discussion	38
4	SECOND HARMONIC GENERATION ENHANCEMENT IN COUPLED PLASMONIC SYSTEMS	45
4.1	Theoretical model examining second harmonic response in coupled plasmonic systems	47
4.2	Experimental evidence of enhancement in second harmonic response of a system of coupled plasmonic oscillators	58
4.2.1	Colloidal solution preparation procedure	59
4.2.2	Optical measurements	60
4.2.3	Experimental results	63
4.3	Summary and Discussion	65
5	CONCLUSIONS	69
	REFERENCES	75
	CURRICULUM VITAE	83

LIST OF TABLES

TABLES

Table 3.1 Lorentz parameters used in computations.	33
--	----

LIST OF FIGURES

FIGURES

Figure 2.1 Schematic representation of surface plasmon polariton oscillations .	6
Figure 2.2 Illustration of the dipole polarizability of a spherical metal nanoparticle under the influence of a plane wave	7
Figure 2.3 A Coupled harmonic oscillator system	11
Figure 2.4 Fano resonance, as the interference of two ionization paths in photoionization process of an atom	12
Figure 3.1 Schematic representation of the model consisting of two coupled plasmonic oscillators	15
Figure 3.2 Real and imaginary parts of the eigenvalues λ_1 and λ_2 , amplitudes of the α_1 and α_2 oscillations	21
Figure 3.3 Lifetimes of the coupled system, with respect to the coupling strength f -1	23
Figure 3.4 Lifetimes of the coupled system, with respect to the coupling strength f -2	24
Figure 3.5 Lifetimes of the coupled system, with respect to the coupling strength f -3	25
Figure 3.6 Lifetimes of the coupled system, with respect to the coupling strength f -4	26
Figure 3.7 Lifetimes of the coupled system, with respect to the coupling strength f -finite integration -1	28
Figure 3.8 Lifetimes of the coupled system, with respect to the coupling strength f -finite integration -2	29
Figure 3.9 Oscillation modes $ \alpha_1 ^2$, $ \alpha_2 ^2$ and $ \alpha_1^{(0)} ^2$ with respect to time . . .	31
Figure 3.10 Illustration of the computational geometry in MEEP calculations .	35

Figure 3.11 Scattering cross sections of the two structures, calculated separately in MEEP	36
Figure 3.12 Normalized energy vs. time results for coupled and uncoupled systems	37
Figure 3.13 Comparison of scattering cross sections	38
Figure 3.14 Comparison of the cases of superposition and coupling of the modes	39
Figure 4.1 A representative picture (a) of the coupled oscillators, and their resonances (b)	49
Figure 4.2 Comparison of the cases with different f_1 s	55
Figure 4.3 Comparison of the cases with different f_2 s	56
Figure 4.4 SHG enhancement for changing values of the coupling f_2	58
Figure 4.5 A darkfield image of the AgNW - AgNP network deposited on microscope cover-slip	59
Figure 4.6 The experimental setup	61
Figure 4.7 a) The absorption spectrum of liquid dispersion of AgNW (black) and a peak fit to the strongest plasmon mode at 390 nm (red). b) The differential absorption curve after the contribution of the strong plasmon peak is subtracted (black), two Gaussian peaks representing the ω_1 , ω_2 (orange solid) plasmon bands.	62
Figure 4.8 A transmission image by the microscope camera on the left and a micro-scan reflection image of the area as indicated by the red rectangle, on the right	63
Figure 4.9 A zoom in into the encircled region in the microscan image along with a sketch of AgNW-AgNP complex	64
Figure 4.10 The SHG spectra	68

LIST OF ABBREVIATIONS

MNS	Metal nanostructure
SHG	Second harmonic generation
SH	Second harmonic
SPP	Surface plasmon polariton
LSP	Localized surface plasmon
LSPR	Localized surface plasmon resonance
FDTD	Finite difference time domain
MEEP	MIT electromagnetic equation propagation
MNS1	Metal nanostructure 1
MNS2	Metal nanostructure 2
PML	Perfectly matched layers
AgNW	Silver nanowire
AgNP	Silver nanoparticle
CW	Continuous wave
PVP	Polyvinylpyrrolidone
EG	Ethylene glycol
NIR	Near infrared
EMCCD	Electron multiplying charge coupled device
SEM	Scanning electron microscope

CHAPTER 1

INTRODUCTION

Light incident on a dielectric surface decorated with metal nanostructures (MNSs) can be trapped and confined into nanoscale sizes. This is a result of interaction of light with collective electron oscillations on MNSs, called surface plasmon polaritons [1, 2]. High intensity induced polarization —provided by strong interaction of incident light with collective charge oscillations around metal nanostructures— leads to various nonlinear optical effects as well as strong interaction among bright and dark modes in the structure. This makes plasmonics attractive for many research areas. Plasmonics is highly engaged in biological sensing [3], optical nanoantennas [4], subwavelength optical imaging [5], fluorescence enhancement [6], plasmonic metamaterials [7], and nonlinear plasmonics [8]. There exist many studies on plasmonic structures regarding linear or nonlinear enhancement in the responses of plasmonic systems [9].

Generation of strong local electromagnetic fields at nanoscale dimensions by surface plasmon polaritons in MNSs is one of the major objectives in plasmonics. Resonant interaction of MNSs with incident optical light can provide a localization of electromagnetic field with 10^5 times higher intensity as compared to the incident field [2, 10]. Despite the strong field intensity of localized plasmons, plasmon lifetime is typically short, most importantly due to radiative (reaction) damping for MNSs larger than 20 nm [11]. As a comparison, semiconductor quantum dots decay with a rate of $10^9 - 10^{11}$ Hz, whereas plasmons decay with that of $10^{13} - 10^{14}$ Hz [10, 12, 13].

Destructive interference of two normal modes results in an asymmetric dip in the spectral response of a coupled system, where otherwise a Lorentzian resonance peak,

at the resonance of the short-lifetime oscillator, is expected to be observed. This phenomenon is called Fano resonance. Fano resonance can improve lifetime of plasmonic oscillations in MNSs. It is observed when two oscillators, one of which has a longer lifetime than the other one, are coupled [14]. The short-lifetime oscillator is driven by a harmonic force, and the absorbed energy rate is governed by the decaying properties of the long-lifetime oscillator. Noginov et. al. 2009, demonstrate a narrowing in the emission spectrum of a Gold nanoparticle core placed in a dye-doped silica shell [12]. Coupling between the Gold nanoparticle and the dye molecules enables the system to respond with a decay rate of the molecular excited level. The new plasmon emission band corresponds to 10^{12} Hz decaying rate, which is much longer than that of the metal nanostructure. This experimental outcome is also theoretically demonstrated [15], as lifetime of plasmonic oscillations can be extended by interacting the metal nanostructures with quantum emitters by Fano resonances. A similar phenomenon is experimentally reported by Sobhani et. al. 2015. They demonstrate that the linewidth in the scattering efficiency of an Aluminium nanoparticle is narrowed as a result of coupling to an Aluminium film, above which the nanoparticle is placed. They also present a theoretical evidence by a model based on multipolar expansion. In plasmonic solar cell applications, improved lifetime of plasmons play a very important role on device efficiency, as light is carried along the photovoltaic structure for longer durations.

In this study, one of the questions addressed theoretically is if a similar lifetime extension can be obtained by an all-plasmonic coupled nanoparticle system. This is the scope of Chapter 3, where a deeper introduction is presented.

Plasmonic nanoantennas could be manufactured to operate more effectively with a good understanding of the Fano-tuned plasmon lifetime mechanism. As well as studies on plasmon lifetime enhancement via Fano resonances, there are experimental demonstrations of lifetime shortening of quantum emitters to obtain ultrafast spontaneous emission [16, 17]. This study can contribute to design process of a plasmonic nanoantenna, as one can make use of the associated results of the theoretical model developed.

One another advantage is the following: It is possible to collect signals and obtain

a decent resolution in the near-field in experiments based on light-matter interactions. However, the measurements are usually performed in the far-field in chemical and bio-sensor applications of plasmonic systems. The presence of dark or long-lived plasmonic modes cannot be detected in the far field so, the effects of these modes cannot be observed and no direct deduction regarding these modes can be obtained [18]. Specifically, if influences of these dark (or long-lived) plasmon modes on scattering cross sections or on time-averaged light-matter interaction were well predictable, designs would be more accurate. In this sense, the theoretical model presented in this study is thought of as a significant contribution to the plasmonics.

Another phenomenon arising out of local field enhancement up to several orders of magnitude by MNSs is that they act as nonlinear conversion agents [19–21]. Strong localized field leads a lot more enhancement in higher harmonic fields compared to the linear responses. This is because, nonlinear responses are proportional to higher order powers of the induced electric field. Enhanced nonlinearity enables MNSs to be utilized as efficient nonlinear converters in many application areas, such as molecular switching, solar energy, photocatalysis, imaging, etc. Optical nonlinearities such as enhanced Raman scattering [22], four wave mixing [23, 24], two photon absorption [25–27], and second harmonic generation (SHG) [28–33] are expected to be detectable only if they are intense enough. Fano resonance mechanism is an effective way to further enhance the nonlinearity over the enhancement due to confinement by MNSs.

It is demonstrated that Fano resonances with attached quantum objects can be beneficial in enhancing [28] and suppressing [20] SHG process in plasmonic particles. The underlying mechanism relies on the cancellation of nonresonant frequency terms (degrading the frequency conversion) by hybridized paths [20]. Fano resonances can also take place in two coupled classical plasmonic oscillators [34, 35], without a quantum nature. It is also experimentally demonstrated that coupling with dark modes (which have longer lifetimes) [36–38] can result in Fano resonances. That is, SHG enhancement in hybrid structures can be obtained even in the absence of coupled quantum emitters. This is an important simplification for facilitating the use of purely metal nanoparticles with appropriate experimental function. By the use of carefully designed metal nanostructures, efficient nonlinear conversion of light can be achieved.

Strongly localized nature of optical conversion can be utilized to address single or few molecules in a background-free fashion.

In chapter 4, a theoretical description of Fano-enhanced SHG in an all-plasmonic coupled systems is presented. It is demonstrated that second harmonic response (SH) findings of the theoretical model applied on a system of two coupled plasmonic oscillators agree well with the experimental study on a similar system including Silver nanoparticles and Silver nanowires.

In this thesis, Fano-coupling of all-plasmonic systems is investigated in terms of linear lifetime enhancement and second harmonic field enhancement. In chapter 3, lifetime of a driven plasmonic oscillator is theoretically explored by two different approaches. The first approach is based on the solution of an eigenvalue problem, treating plasmon fields as quantum harmonic oscillators in the Heisenberg picture. In the second approach the system is treated as an electromagnetic problem and the Maxwell's equations are numerically solved to obtain total electromagnetic energy around a plasmonic structure in time. Relying on the agreement of the results of both approaches, it is theoretically demonstrated that lifetime of a driven plasmonic oscillator is enhanced by attaching it to another plasmonic oscillator, lifetime of which is shorter than that of the driven one. In chapter 4, in the first part, a theoretical model describing the SH response of an all-plasmonic coupled system is presented. In the second part, an experimental study, results of which are predicted well by the theoretical model is reported. The experimental and the theoretical results agree well with each other and demonstrate that SH field arising from a driven plasmonic structure is enhanced by attaching it to another plasmonic structure with longer lifetime. Both linear lifetime enhancement, and SH field enhancement rely on Fano resonances, as the cases explored in both chapters are manifestations of the phenomenon that is characterized as follows: The short-lifetime oscillator is driven by an harmonic force, and the absorbed energy rate is governed by the decaying properties of the long-lifetime oscillator.

CHAPTER 2

THEORETICAL BACKGROUND

In this chapter a brief introduction to plasmonics and Fano resonance is presented.

2.1 Plasmonic oscillations

The discovery of collective charge oscillations dates back over one century with Wood's anomalies, manifesting itself as intensity drops in optical reflection spectra of metallic diffraction gratings. Although Wood was unable to provide any interpretation to these phenomena [39], he is considered as the initiator of plasmonics. Rayleigh and Fano proposed the first theoretical explanations to the experimental observations of Wood without stating surface plasmon excitations [40–42]. The invention of lasers provided the modern analysis of these anomalies. In 1957, Ritchie [43] attributed energy losses of fast electrons partly to collective interactions in thin metal films, and the term surface plasmons is first stated by Stern and Ferrel [44], referred as the collective oscillations of free electrons in noble metals.

Plasmon is the quasiparticle of the collective oscillations of free electrons in noble metals. There are types of plasmonic excitations that are distinguished by the geometry of metals on which the collective charge oscillations are excited. In large volumes of metal structures, plasmon oscillations can exist in bulk modes, called bulk plasmons or volume plasmons. Plasmon oscillations can be excited in such a way that they propagate evanescently at the interfaces between dielectric and metal structures. These type of oscillations are called surface plasmon polaritons (SPPs). Small size metal structures such as nanoparticles can support localized surface plasmons (LSPs)

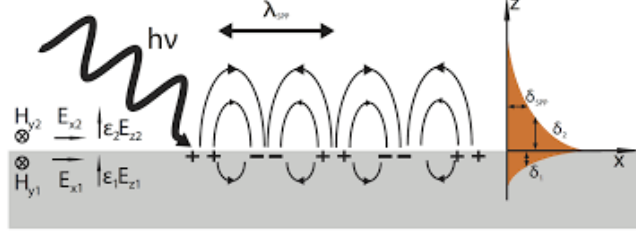


Figure 2.1: Schematic representation of surface plasmon polariton oscillations. Electric and magnetic components are given as well as the decay lengths into both materials.

in the near field.

2.1.1 Surface plasmon polaritons

There exist propagating solutions of Maxwell's equations at metal-dielectric interfaces, called surface plasmon polaritons. These are dispersive longitudinal waves propagating along the interface, decaying exponentially into both media. Typical decay lengths are a few tens of nanometres into the metal and few hundreds of nanometres into the dielectric. The solution of Maxwell's equations provide the dispersion relation as follows,

$$k_{\text{SPP}} = \frac{\omega}{c} \sqrt{\frac{\epsilon_d \epsilon_m}{\epsilon_d + \epsilon_m}}, \quad (2.1)$$

ϵ_d and ϵ_m being the permittivities of dielectric and metal, respectively. The schematic representation of surface plasmon polaritons is shown in Fig. 2.1. Charge density propagates along z direction, associated with an evanescent field decaying into metal and dielectric media, with the decay rates shown in the z - x graph in Fig. 2.1. Surface plasmon polaritons can be excited very efficiently with light in the visible range of the electromagnetic spectrum by several different mechanisms such as the ones performed by Otto [45] and Kretschmann [46], and grating configurations which rely on momentum conserved evanescent (Otto) or dispersion allowed (Kretschmann) zone folded (grating) coupling.

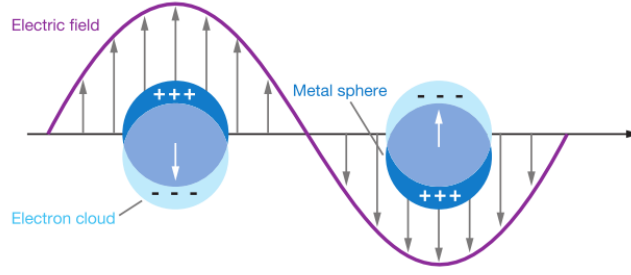


Figure 2.2: Illustration of the dipole polarizability of a spherical metal nanoparticle under the influence of a plane wave. *Adopted from Ref. [47].*

2.1.2 Localized surface plasmons

Localized surface plasmons are the nonpropagating counterpart of SPPs, which can be excited at the nanoscale subwavelength metallic structures. In metallic nanostructures, free electron density oscillating around fixed positive ions back and forth under the influence of Coulomb's force, can be resonantly excited by electromagnetic fields at frequencies where the polarizability is strongly enhanced [47]. Due to enhanced polarizabilities, light is confined into nanoscale sizes leading to enhanced near fields in the vicinity of the nanostructures, called hotspots. Fig. 2.2 shows a schematic representation of LSP oscillations.

The condition for localized surface plasmons to be excited is called localized surface plasmon resonance (LSPR). Scattering of an electromagnetic plane wave by a homogeneous sphere has already been treated by Mie in the early 1900's. LSPR condition for the case of a metal sphere, size of which is much smaller than the source wavelength can be obtained by analytical solutions of Maxwell's equations. Considering the problem in the regime where the size of the particle is small, allows one to treat the problem in the quasistatic approximation in which the retardation effects are neglected by assuming the electric field over the nanostructure to be constant. However, the permittivity of the metal and the medium is still frequency dependent. LSPR condition is derived by Laplace equation,

$$\nabla^2 \phi = 0. \quad (2.2)$$

Then, the electric field is calculated as

$$\mathbf{E} = -\nabla\phi. \quad (2.3)$$

The boundary conditions are required that both normal and tangential components of the electric field at the interface between the metal nanoparticle and the surrounding medium are continuous. Then, the solution for the electric field of the metal nanosphere is calculated to be a superposition of the incident field and the dipole moment due to the metal sphere. The resonance condition follows from the calculated complex polarizability of the metal nanosphere:

$$\alpha = 4\pi R^3 \frac{\epsilon_p - \epsilon_m}{\epsilon_p + 2\epsilon_m}, \quad (2.4)$$

where ϵ_p and ϵ_m are permittivities of the particle and the medium, respectively. When the denominator of the expression given in Eq. (2.4) is vanished, the condition for the excitation of the dipolar resonance mode in the metal nanosphere is satisfied. The information of damping of the plasmon oscillations is carried by the magnitude of the imaginary part of the permittivity. This condition is obtained in the quasistatic limit and hence the spectral position of the plasmon resonance is independent on the size of the nanoparticle, which is not usually true. For nanoparticles with larger and/or more complex geometries, quasistatic limit does not work any more. Because retardation effects come into play and these kind of structures may support higher order modes. Higher order modes, such as quadrupole, octupole, and etc., typically display narrower linewidths and/or smaller scattering cross sections.

2.2 Nonlinear plasmonics

The ability of metal nanostructures to confine light into nanoscale sizes opens up light controlling opportunities at the nanoscale. Since the resulting electromagnetic field is very strong, it is possible to observe nonlinear effects. Plasmonic structures can be utilized to reveal nonlinearities on linear dielectric structures. There exist studies on nonlinear plasmonics where plasmonic structures are used as nonlinear frequency

converters, to switch and modulate optical signals, and to reveal soliton effects [8].

Frequency conversion is a nonlinear process, where it is provided that the frequency of the response field is different than that of the incident field; it is converted into some different frequency obeying conservation of energy. Sum-difference frequency generations, second (and higher order) harmonic generations are examples of frequency conversion processes.

2.2.1 Second harmonic generation

Second harmonic generation is a nonlinear optical process where interaction of photons results in annihilation of two photons of the same frequency, and creation of a single photon with twice the frequency. It is an even-order nonlinear process and hence allowed only in non-centrosymmetric media. It is a special case of sum frequency generation.

Optical response of a linear medium is determined by the following linear relation,

$$\mathbf{P} = \epsilon_0 \chi^{(1)} \mathbf{E}, \quad (2.5)$$

where \mathbf{P} is the polarization density (response), ϵ_0 is the electric permittivity of the free space, $\chi^{(1)}$ is the linear electric susceptibility, and \mathbf{E} is the electric field (source). Both fields oscillate with the same frequency, ω . For a nonlinear material, the optical response can be expressed as the Taylor expansion of polarization \mathbf{P} , in powers of \mathbf{E} ,

$$P_k = \epsilon_0 (\chi_{ik}^{(1)} E_i + \chi_{ijk}^{(2)} E_i E_j + \chi_{ijkl}^{(3)} E_i E_j E_l + \dots), \quad (2.6)$$

where P_k is one of the three spatial components of the nonlinear polarization, i.e., $k = x, y, z$, and Einstein's summation convention is used. $\chi^{(n)}$ is the susceptibility tensor of n^{th} order nonlinear process. In this expression, the first term is the linear response of the material, identical to the vectorial expression given in Eq. (2.5), and higher order terms correspond to higher order responses, oscillating with frequencies,

2ω , 3ω , and etc. When the incident electric field, that is expressed as

$$E_i = \epsilon_i e^{-i\omega t} + \epsilon_i^* e^{+i\omega t}, \quad (2.7)$$

is substituted into Eq. (2.6), the second term becomes

$$P_{k,2} = \chi_{ijk}^{(2)} (\epsilon_i \epsilon_j e^{-2i\omega t} + \epsilon_i^* \epsilon_j^* e^{+2i\omega t} + \epsilon_i \epsilon_j^* + \epsilon_i^* \epsilon_j). \quad (2.8)$$

Here, last two terms are referred as optical rectification corresponding to a DC electrical field. Second harmonic response of the system is the radiation with frequency 2ω which is represented by the first two terms.

2.3 Fano resonance

A resonance is usually referred to an enhancement in the response of a system to an external source that excites the system at a certain frequency. This frequency is referred as the natural frequency of the system. The simplest example is a harmonic oscillator driven by a periodic force. When the frequency of the periodic force is close to the frequency of the eigenmode of the oscillator, than the amplitude of the oscillator displays a maximum. An opposite effect can be observed in a system when the harmonic oscillator is coupled with another one having a smaller damping rate. The response of the driven oscillator exhibits two maxima, one of which has the usual Lorentzian shape at the natural frequency of the driven oscillator. The second resonance is observed at the natural frequency of the harmonic oscillator with a smaller damping. At this frequency, the resonance displays an asymmetric sharp dip where the amplitude drops to zero, as shown in Fig. 2.3b. The reason for such a response is because at this frequency, the first harmonic oscillator is effectively under the influence of two driving forces that are out of phase, and hence cancel each other. In other words, oscillations from the external force and the coupled oscillator destructively interfere. These results are obtained by solving the coupled differential equations of the harmonic oscillators with a periodic force, details of which can be found is Ref. [48]. Such an asymmetric shape in the response of the driven oscillator in a coupled system

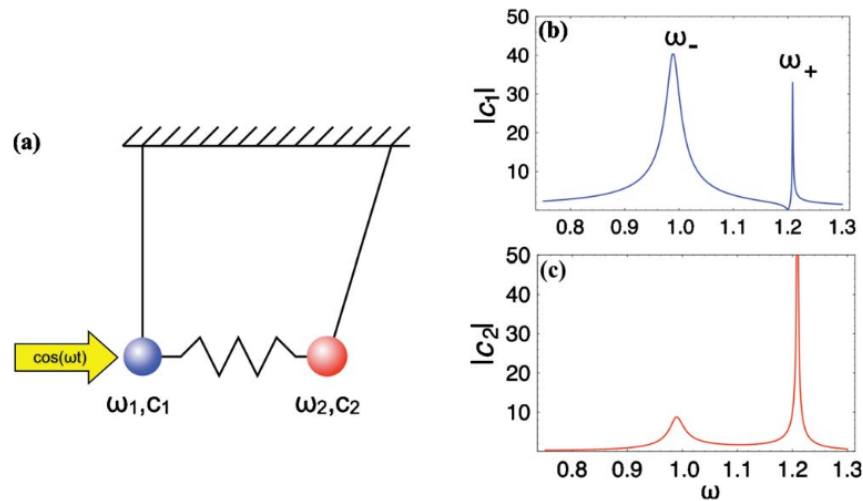


Figure 2.3: A Coupled harmonic oscillator system. (a) Schematic representation of two coupled oscillators, one of which is driven by the driving field, with given natural frequencies, and amplitudes. Responses of the forced (b) and the coupled (c) oscillators. Forced oscillator displays two resonances; a symmetric and an asymmetric profiles around the eigenfrequencies ω_1 and ω_2 . The second oscillator displays symmetric resonance profiles at the same spectral positions. *Adopted from Ref. [14].*

is referred as Fano resonance.

Fano [49, 50] was the one who first prove a theoretical explanation to such unusual resonance profiles observed by Beutler [51]. The term Fano resonance was first used to describe the asymmetric resonance profiles observed in the spectrum of scattering electrons, as a result of destructive interference between continuum and discrete atomic states observed in photoionization processes. The classical analog of this phenomenon is explained above. The original Fano resonance is a quantum effect and is observed in photoionization process of electrons. An electron can be directly excited from a deep inner shell to above the ionization threshold energy level which can be considered as the straightforward way of photoionization. The excited state is a continuum. An alternative way is autoionization, where two electrons are excited by one photon, and as a result of interaction between these electrons, one of the electrons falls to a lower energy state whereas the other is ejected into the continuum consuming the energy of the relaxed electron. This phenomenon is also known as the Auger effect. Fig. 2.4 illustrates these ionization possibilities. Quantum superposition of these possibilities allows coupling between these two paths leading to interferences.

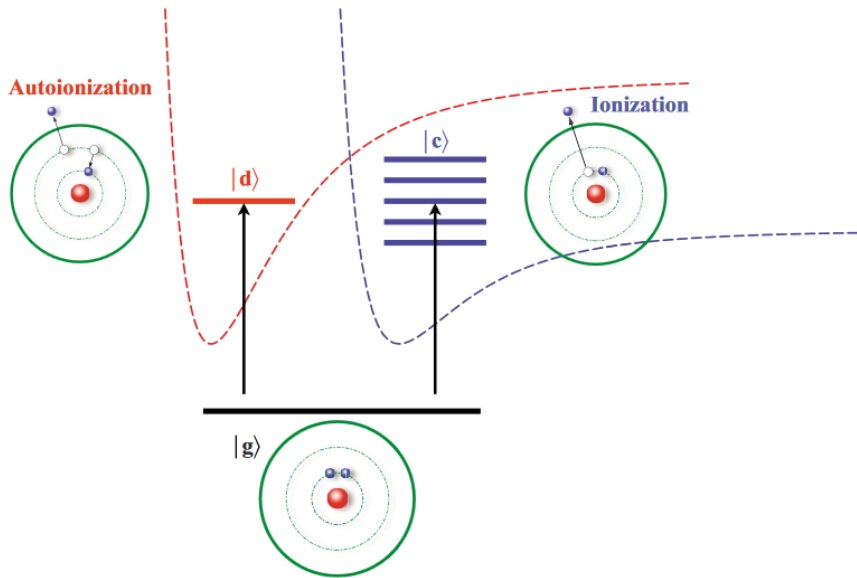


Figure 2.4: Fano resonance is described as the interference of two ionization paths in photoionization process of an atom: i) an electron can directly be ionize from a deep inner-shell or ii) two lectrons can be excited by autoionization (Auger process). This processes can be considered as a transition of an electron from the ground state $|g\rangle$ to a continuum $|c\rangle$ or a discrete autoionized state $|d\rangle$. *Adopted from Ref. [14].*

Fano explained unusual sharp asymmetric dips observed in the resonance profiles in the scattering response of electrons by Buetler by using these arguments and obtained a formula for the shape of such resonance profiles starting from a perturbative approach.

CHAPTER 3

LIFETIME ENHANCEMENT IN COUPLED PLASMONIC SYSTEMS

Lifetime of plasmonic oscillations in metal nanostructures can be extended by a phenomenon called Fano resonance. It arises from the interferences of phase-varying multiple paths of absorption, observed when two oscillators, one of which has a narrower linewidth than the other, are coupled. A narrower linewidth corresponds to a longer lifetime. It is theoretically presented [15] that it is possible to extend the lifetime of plasmonic oscillations by making the metal nanostructures interact with quantum emitters at certain frequencies, introducing Fano resonances. Noginov et. al. 2009, experimentally demonstrate a narrowing in the emission spectrum of a Gold nanoparticle core placed in a dye-doped silica shell [12]. Coupling between the Gold nanoparticle and the dye molecules enables the system to respond with a decay rate of the molecular excited level. In this chapter, the question "if one can obtain a similar extension when the plasmonic oscillators are coupled to the long lived plasmonic dark states" is raised. A dark state refers to a state of an atom or molecule that can not absorb or emit photons [52]. A plasmonic dark state is a long-lived excitation that cannot be excited by an incident field. The overlap integral

$$f_{dark} \propto \int E_1^*(\mathbf{r})E_2(\mathbf{r})d^3\mathbf{r}$$

describing the interaction between an incident field, $E_1(\mathbf{r})$, and an atomic state, $E_2(\mathbf{r})$, vanishes due to even/odd symmetries for the case of interaction between an incident field and a dark state. However a dark state can couple to (be excited by)

near-field polarization of an excited bright plasmon mode. When a system consists of plasmonic structures with modes, resonant to a source field, this field can be confined into nanoscale dimensions, and interact with long-lived dark states. Lifetime of plasmons are typically small (in the order of 10 - 100 fs), that is small compared to that of quantum emitters (in the order of ns to ps) which are not as convenient as larger particles in the range from a few to a few hundred nanometers to be used in optical systems. Besides, molecules have limited exposure times. Another advantage of plasmonic dark states over atomic states is that interaction between a plasmonic mode and an atom cannot be as strong as interaction between two plasmonic modes. This follows from the comparison of overlap integrals of both cases.

It is shown that coupling short lifetime particles with longer lifetime ones provides confinement of light with nanoscale dimensions for longer durations. The extension of plasmon lifetime is demonstrated by two different approaches. The first approach relies on a very basic analytical analysis of the problem, and proves that the lifetime is enhanced via path interference effects. In this approach, plasmon polarization fields are treated as harmonic oscillations. Two plasmonic structures are considered. One can be excited resonantly by an incident light. The other nanostructure cannot be excited directly by the incident field, but supports a long-lived dark state. The coupled system is initiated so that the plasmonic excitation is only on the driven nanoparticle, and the time evolution of the total number of plasmons is observed in the coupled system. The analytical solution of the eigenvalue equation for the simplest coupling scenario provides evidence for lifetime enhancement. The second approach is based on numerical solutions of 3D Maxwell's equations. A three dimensional system is illuminated by a Gaussian pulse of a sharp frequency width, and electromagnetic energy of a metal nanoparticle, on which oscillation lifetime is desired to be enhanced is observed in time.

3.1 Eigenvalue problem of a coupled plasmonic system

In this section, the lifetime of plasmonic oscillations is examined within a simple coupled harmonic oscillator model. The lifetime of the plasmonic oscillations is examined for varying values of the coupling strength, f .

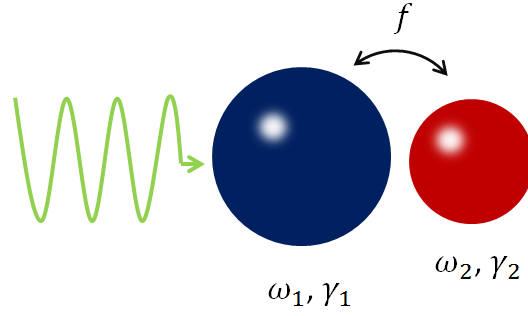


Figure 3.1: Two plasmonic oscillators are coupled. The strength of coupling between the particles is determined by coefficient f , in units of frequency. Frequencies and the damping rates are given. The particle with resonance frequency ω_1 is driven by the incident field and has a shorter lifetime ($\gamma_1 \gg \gamma_2$) compared to the second particle which supports a dark state. The lifetime of the coupled system is examined for varying f .

The model system consists of two interacting harmonic oscillators, corresponding to two quantized plasmon modes in two metal nanoparticles. The plasmonic oscillator with short lifetime supports a mode, that is resonant with the incident field. Coupling this plasmonic oscillator with the second one of a longer lifetime, it is expected to enhance the polarization durations on the coupled plasmonic oscillators, by introducing path interferences. The plasmonic oscillator that is attached to the driven oscillator cannot be excited by the pump field directly. The plasmonic oscillation modes, the driven and the dark mode, are described by amplitudes $\alpha_1^{(0)}$, $\alpha_2^{(0)}$ and associated with natural frequencies ω_1 , ω_2 , and damping rates, γ_1 , γ_2 , respectively. In the absence of the coupling between the two particles, the eigenmodes are

$$\alpha_1^{(0)}(t) \propto e^{-(i\omega_1 + \gamma_1)t} \quad (3.1)$$

$$\alpha_2^{(0)}(t) \propto e^{-(i\omega_2 + \gamma_2)t}. \quad (3.2)$$

Number of plasmons in a plasmonic oscillator is defined by the absolute square of oscillation amplitude. Then, the total number of plasmons on the two particles in the absence of coupling is defined as

$$N^{(0)}(t) = |\alpha_1^{(0)}(t)|^2 + |\alpha_2^{(0)}(t)|^2. \quad (3.3)$$

Since α_2 oscillations cannot be driven directly by the pump field, and there is no interaction between the particles, only α_1 mode contributes to the total number of plasmons in Eq. 3.3. When the two particles are brought together, the modes are hybridized and there are contributions from oscillations on both particles. In the model system, shown in Fig. 3.1, the interaction between oscillators is defined by a parameter f , in the dimension of frequency. The model to be described in this section is a dimensionless model, assuming the frequency of the pump field to be $\omega = 1$. That follows, any frequency or damping is treated as a factor of $\omega = 1$, and time as a factor of $1/\omega$, which is also 1. In the physical situation, a nonzero f corresponds to a case when the two metal nanoparticles are brought together; close enough for the polarization fields induced on the particles to overlap and hence interact. The interaction between particles is expected to introduce Fano resonances at certain frequencies, enhancing the oscillation durations of the plasmons. When there is a nonzero coupling between the structures, new solutions of the oscillations are hybridized. The solutions are in the form of linear combinations of the two new oscillation modes, as

$$\alpha_1(t) \propto e^{h_1(\omega_1, \omega_2, \gamma_1, \gamma_2, f)t} + e^{h_2(\omega_1, \omega_2, \gamma_1, \gamma_2, f)t}, \quad (3.4)$$

$$\alpha_2(t) \propto e^{g_1(\omega_1, \omega_2, \gamma_1, \gamma_2, f)t} + e^{g_2(\omega_1, \omega_2, \gamma_1, \gamma_2, f)t}. \quad (3.5)$$

Here, the functions appearing on the exponents depend on the parameters of the system. The total number of plasmons in the system is defined as

$$N(t) = |\alpha_1(t)|^2 + |\alpha_2(t)|^2. \quad (3.6)$$

Lifetime of the coupled system is defined using $N(t)$ in Eq. (3.29) The lifetime of the coupled system with varying coupling, f is calculated. The problem is treated as an eigenvalue problem, with a 2×2 matrix of equations of motions derived from the Hamiltonian

$$\hat{H} = \hbar\omega_1\hat{a}_1^\dagger\hat{a}_1 + \hbar\omega_2\hat{a}_2^\dagger\hat{a}_2 + \hbar(f\hat{a}_1^\dagger\hat{a}_2 + f^*\hat{a}_1\hat{a}_2^\dagger) + i\hbar(\hat{a}_1^\dagger\epsilon_p e^{-i\omega t} + \text{H. c.}). \quad (3.7)$$

where \hat{a}_1 and \hat{a}_2 are the annihilation operators for the collective plasmon excitations in the driven and the attached oscillators, corresponding to the modes with resonance frequencies ω_1 and ω_2 , respectively. Since properties like entanglement are not of interest, they will soon represent the amplitudes of the associated plasmon oscillations. f is the coupling matrix element between the polarization field induced by \hat{a}_1 , mode of the driven oscillator, and \hat{a}_2 , mode of the attached oscillator. The first and the second terms on the right hand side of Eq. (3.7) are the energy operators of the two oscillation modes, the third term corresponds to the interaction energy, and the last term corresponds to the coupling of the pump to the driven oscillator, \hat{a}_1 .

In quantum mechanics, for any observable \hat{A} , the dynamics is described by the Heisenberg equation,

$$i\hbar \frac{d\hat{A}}{dt} = [\hat{A}(t), \hat{H}] + \left(\frac{\partial \hat{A}}{\partial t}\right)_H. \quad (3.8)$$

Heisenberg equations for the operators \hat{a}_1 and \hat{a}_2 are obtained by substituting them in Eq. (3.8).

$$\dot{\hat{a}}_1 = -i\omega_1 \hat{a}_1 - if \hat{a}_2 + \epsilon_p e^{-i\omega t} \quad (3.9)$$

$$\dot{\hat{a}}_2 = -i\omega_2 \hat{a}_2 - if^* \hat{a}_1 \quad (3.10)$$

Damping of the plasmon modes is not included in the Hamiltonian, so the damping rates γ_1 and γ_2 are plugged in the equations. The term for the driving force is removed, since the decay time of the coupled system where the driven oscillator is initiated from the excited state, is of interest. The followings are the equations of motion describing the dynamics of the coupled plasmonic oscillator system.

$$\dot{\alpha}_1 = -(i\omega_1 + \gamma_1)\alpha_1 - if\alpha_2 \quad (3.11)$$

$$\dot{\alpha}_2 = -if^*\alpha_1 - (i\omega_2 + \gamma_2)\alpha_2 \quad (3.12)$$

The eigenvalue equation is

$$M\alpha = \lambda\alpha. \quad (3.13)$$

Here α is the 2×1 amplitude vector,

$$\alpha = \begin{pmatrix} \alpha_1 \\ \alpha_2 \end{pmatrix}, \quad (3.14)$$

and the 2×2 matrix M is given by

$$M = \begin{pmatrix} -a & -if \\ -if & -b \end{pmatrix}, \quad (3.15)$$

where

$$\begin{aligned} a &= (i\omega_1 + \gamma_1) \\ b &= (i\omega_2 + \gamma_2) \end{aligned}, \quad (3.16)$$

and f is real. The degree of freedom is reduced to one by taking f real because in this section, obtaining the simplest and the quickest evidence of lifetime enhancement is aimed. The eigenvalues and the eigenvectors are found as

$$\lambda_{1,2} = \frac{1}{2}(-a - b \pm \sqrt{(a + b)^2 - 4ab - 4f^2}), \quad (3.17)$$

$$\alpha^{(1)} = \begin{pmatrix} \frac{-if}{\sqrt{f^2 + (a + \lambda_1)^2}} \\ \frac{a + \lambda_1}{\sqrt{f^2 + (a + \lambda_1)^2}} \end{pmatrix}, \quad \alpha^{(2)} = \begin{pmatrix} \frac{-if}{\sqrt{f^2 + (a + \lambda_2)^2}} \\ \frac{a + \lambda_2}{\sqrt{f^2 + (a + \lambda_2)^2}} \end{pmatrix}. \quad (3.18)$$

So the general solution is

$$\alpha(t) = c_1\alpha^{(1)}e^{\lambda_1 t} + c_2\alpha^{(2)}e^{\lambda_2 t}, \quad (3.19)$$

or more explicitly,

$$\alpha_1(t) = c_1 \frac{-if}{\sqrt{f^2 + (a + \lambda_1)^2}} e^{\lambda_1 t} + c_2 \frac{-if}{\sqrt{f^2 + (a + \lambda_2)^2}} e^{\lambda_2 t}, \quad (3.20)$$

$$\alpha_2(t) = c_1 \frac{a + \lambda_1}{\sqrt{f^2 + (a + \lambda_1)^2}} e^{\lambda_1 t} + c_2 \frac{a + \lambda_2}{\sqrt{f^2 + (a + \lambda_2)^2}} e^{\lambda_2 t}, \quad (3.21)$$

where c_1 and c_2 are the coefficients to be determined from the initial conditions. The incident field is introduced and drives the plasmonic mode that is supported by the metal nanoparticle with shorter lifetime, and then it is turned off. It is assumed that, initially there are only α_1 oscillations. So the initial conditions are given by

$$\alpha_1(0) = 1, \quad \alpha_2(0) = 0. \quad (3.22)$$

Applying the initial conditions given in Eq. (3.22), the solution is found as

$$\alpha_1(t) = \frac{a + \lambda_2}{\lambda_2 - \lambda_1} e^{\lambda_1 t} - \frac{a + \lambda_1}{\lambda_2 - \lambda_1} e^{\lambda_2 t}, \quad (3.23)$$

$$\alpha_2(t) = -\frac{(a + \lambda_1)(a + \lambda_2)}{if(\lambda_2 - \lambda_1)} e^{\lambda_1 t} + \frac{(a + \lambda_1)(a + \lambda_2)}{if(\lambda_2 - \lambda_1)} e^{\lambda_2 t}, \quad (3.24)$$

where $\lambda_{1,2}$ are given in Eq. (3.17). For brevity, substituting,

$$\begin{aligned} A_1 &= \frac{a + \lambda_2}{\lambda_2 - \lambda_1}, & B_1 &= -\frac{a + \lambda_1}{\lambda_2 - \lambda_1}, \\ A_2 &= -\frac{(a + \lambda_1)(a + \lambda_2)}{if(\lambda_2 - \lambda_1)}, & B_2 &= -A_2, \end{aligned} \quad (3.25)$$

the solutions have the form

$$\alpha_1(t) = A_1 e^{\lambda_1 t} + B_1 e^{\lambda_2 t}, \quad (3.26)$$

$$\alpha_2(t) = A_2 e^{\lambda_1 t} + B_2 e^{\lambda_2 t}. \quad (3.27)$$

The total number of plasmons for the most general case is given by Eq. (3.6). Substituting the solutions of the eigenvalue problem given in Eq.s (3.26,3.27) into Eq. (3.6), the total number of plasmons in a coupled system of two plasmonic oscillators is found as follows

$$\begin{aligned}
N(t) = & [|A_1|^2 + |A_2|^2]e^{2\Re(\lambda_1)t} + [|B_1|^2 + |B_2|^2]e^{2\Re(\lambda_2)t} \\
& + [A_1B_1^* + A_2B_2^*]e^{\{\Re(\lambda_1)+\Re(\lambda_2)+i[\Im(\lambda_1)-\Im(\lambda_2)]\}t} \\
& + [A_1^*B_1 + A_2^*B_2]e^{\{\Re(\lambda_1)+\Re(\lambda_2)+i[-\Im(\lambda_1)+\Im(\lambda_2)]\}t}, \quad (3.28)
\end{aligned}$$

where \Re and \Im stands for real and imaginary parts of the complex expressions.

3.1.1 Long term behaviour of the plasmon decay

The lifetime of the plasmon polarization oscillations, τ , can be defined as the mean value of the time weighted over plasmon intensity.

$$\tau = \frac{\int_0^\infty t N(t) dt}{\int_0^\infty N(t) dt} \quad (3.29)$$

Fig. 3.2 shows real and imaginary parts of the eigenvalues λ_1 and λ_2 , corresponding to the oscillation damping rates, (a) and frequencies, (b) respectively, and the amplitudes of both oscillations separately (c,d), for varying values of the coupling strength f . Oscillation parameters are set to $\omega_1 = 1.0, \omega_2 = 1.8, \gamma_1 = 0.1, \gamma_2 = 0.01$. Evaluating these figures, one can say that it is possible to tune the lifetime of the oscillations by choosing an appropriate coupling, f , between the particles. As the decay rates and the amplitudes change with the amount of coupling, an optimal coupling can be set to introduce constructive interference to enhance the oscillation duration.

Substituting Eq. (3.28) into Eq. (3.29), it is found that

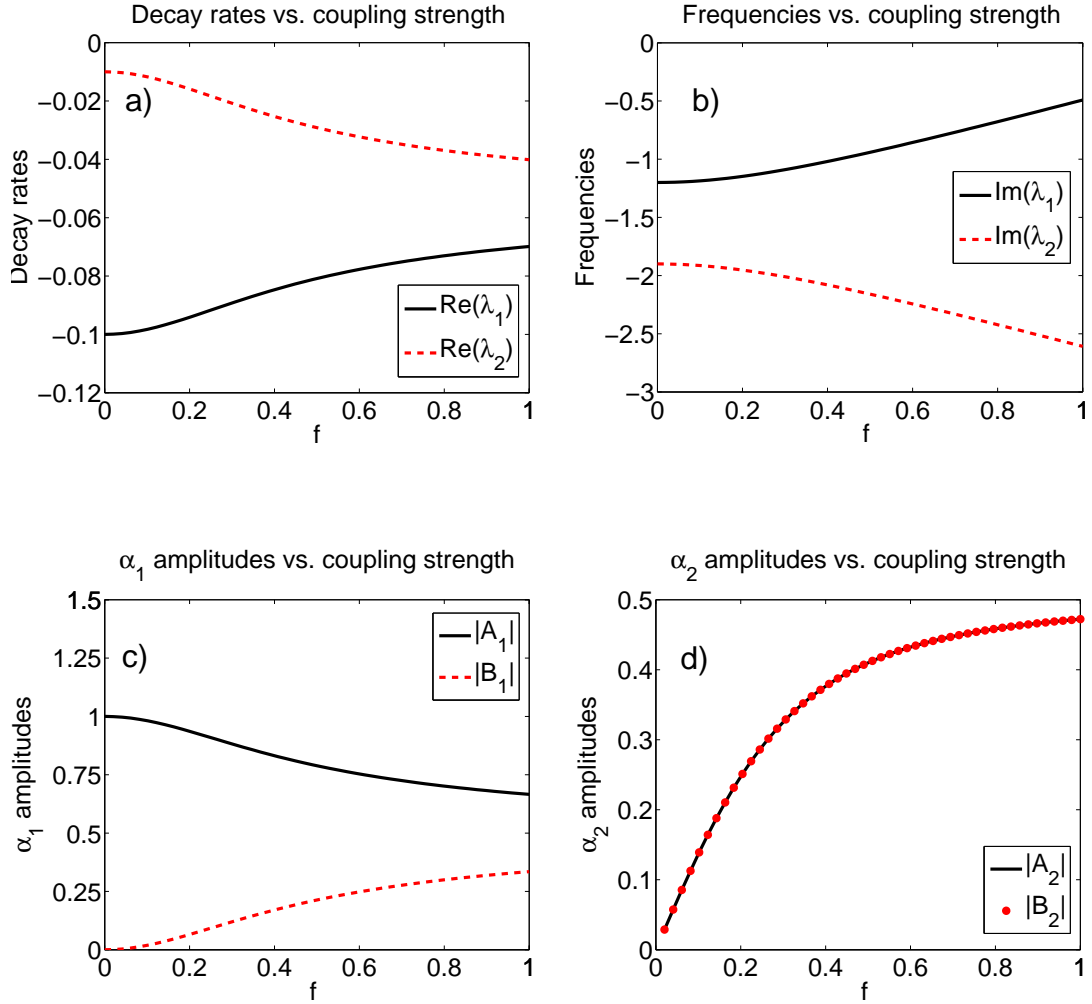


Figure 3.2: Real and imaginary parts of the eigenvalues λ_1 and λ_2 , corresponding to the damping rates (a) and the frequencies (b) of the oscillations of the coupled system, respectively. Amplitudes of the α_1 and α_2 oscillations in Eq.s (3.26-3.27); $|A_1|, |B_1|$ (c), and $|A_2|, |B_2|$ (d), respectively. Parameter set is $\omega_1 = 1.0, \omega_2 = 1.8, \gamma_1 = 0.1, \gamma_2 = 0.01$. The quantities are dimensionless.

$$\begin{aligned}
\int_0^\infty N(t) dt &= -\frac{|A_1|^2 + |A_2|^2}{2\lambda_1} - \frac{|B_1|^2 + |B_2|^2}{2\lambda_2} \\
&\quad - \frac{A_1 B_1^* + A_2 B_2^*}{\Re(\lambda_1) + \Re(\lambda_2) + i[\Im(\lambda_1) - \Im(\lambda_2)]} \\
&\quad - \frac{A_1^* B_1 + A_2^* B_2}{\Re(\lambda_1) + \Re(\lambda_2) + i[-\Im(\lambda_1) + \Im(\lambda_2)]}, \tag{3.30}
\end{aligned}$$

and

$$\begin{aligned}
\int_0^\infty t N(t) dt &= \frac{|A_1|^2 + |A_2|^2}{4[\Re(\lambda_1)]^2} + \frac{|B_1|^2 + |B_2|^2}{4[\Re(\lambda_2)]^2} \\
&\quad + \frac{A_1 B_1^* + A_2 B_2^*}{\{\Re(\lambda_1) + \Re(\lambda_2) + i[\Im(\lambda_1) - \Im(\lambda_2)]\}^2} \\
&\quad + \frac{A_1^* B_1 + A_2^* B_2}{\{\Re(\lambda_1) + \Re(\lambda_2) + i[-\Im(\lambda_1) + \Im(\lambda_2)]\}^2}. \tag{3.31}
\end{aligned}$$

Eq.s (3.30,3.31) are substituted into Eq. (3.29) to obtain the oscillation lifetimes of the coupled system for different coupling strengths, f . In this treatment, lifetime of the coupled system is defined by Eq. (3.29), and depends on the parameters of the particles, namely, $\omega_1, \omega_2, \gamma_1$, and γ_2 . These parameters are fixed. The only variable in the calculations is the parameter determining the coupling strength, i.e., f . For the most general case, f is a complex number in units of frequency but it is assumed to be real in order to obtain the simplest outcome from this model. For different parameter sets, effective oscillation durations of the plasmons are obtained. The results are shown in Fig.s 3.3-3.6. These results are obtained from analytical solutions of the integrations in Eq. (3.29). The same results are also obtained, thereby confirmed by numerical integrations of the same equation in MATLAB.

The results shown in Fig.s 3.3-3.6 are obtained from a theoretical model based on the solutions of Heisenberg equations of the oscillation modes in a coupled plasmonic system consisting two plasmonic oscillators, one of which is driven by an incident field and supports short lifetime oscillations, coupled with an attached plasmonic oscillator, supporting longer lifetime oscillations. Fig.s 3.3-3.6 demonstrates the lifetime vs. coupling strength for different oscillation parameter sets, given on each graph. The lifetime of the coupled system is defined by Eq. (3.29). This equation does not consist of any information about the incident driving field, since the

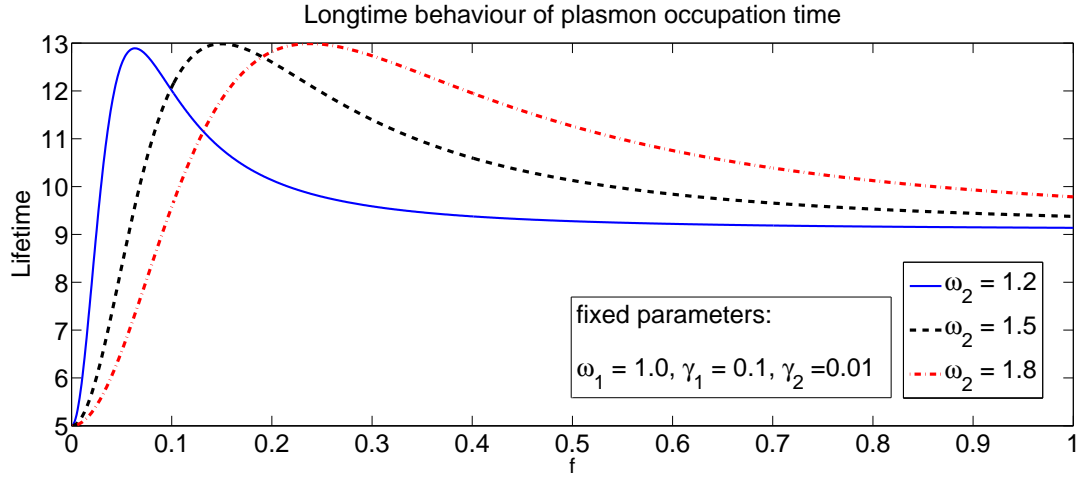


Figure 3.3: Lifetimes of the coupled system, τ , calculated from Eq. (3.29), with respect to the coupling strength f . The resonance frequency of the driven oscillator is set to $\omega_1 = 1.0$ and the resonance frequency of the dark mode, ω_2 , is assigned to different values. Damping rates are set to $\gamma_1 = 0.1, \gamma_2 = 0.01$. The enhancement factor is found as 2.6, at the coupling strengths $f = 0.066, f = 0.150, f = 0.240$, for $\omega_2 = 1.2, \omega_2 = 1.5, \omega_2 = 1.8$, respectively. As the detuning between the resonance frequencies of the oscillators is increased, a stronger coupling is required to obtain the same lifetime enhancement. The quantities are dimensionless.

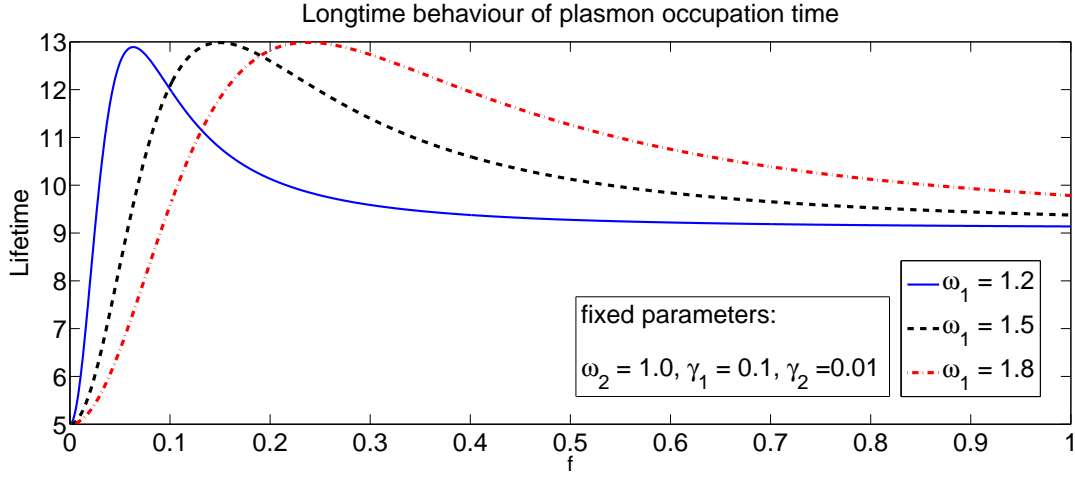


Figure 3.4: Lifetimes of the coupled system, τ , calculated from Eq. (3.29), with respect to the coupling strength f . The resonance frequency of the dark mode is set to $\omega_2 = 1.0$ and the resonance frequency of the driven oscillator, ω_1 , is assigned to different values. Damping rates are set to $\gamma_1 = 0.1, \gamma_2 = 0.01$. The enhancement factor is found as 2.6, at the coupling strengths $f = 0.066, f = 0.150, f = 0.240$, for $\omega_1 = 1.2, \omega_1 = 1.5, \omega_1 = 1.8$, respectively. As the detuning between the resonance frequencies of the oscillators is increased, a stronger coupling is required to obtain the same lifetime enhancement. Comparing these results with the ones shown in Fig. 3.3, a symmetry between the resonance frequencies of the oscillators is observed. The quantities are dimensionless.

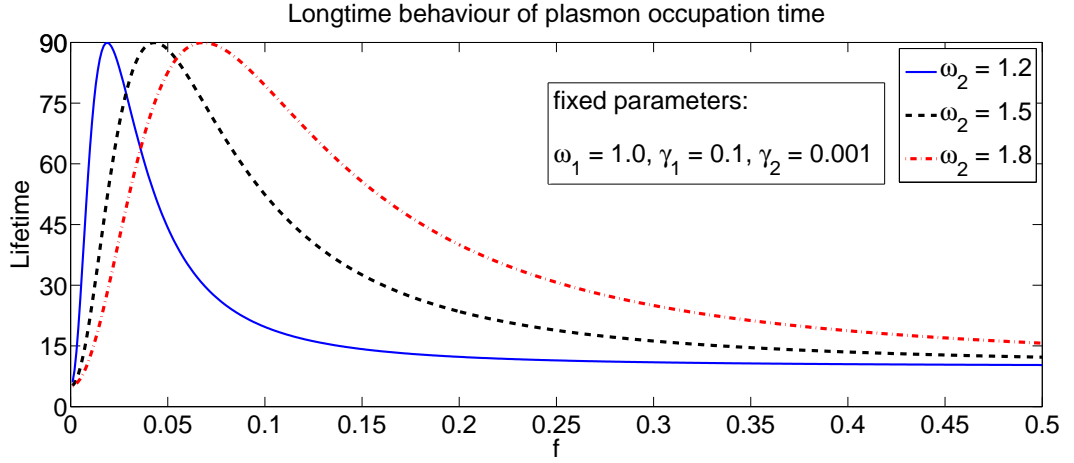


Figure 3.5: Lifetimes of the coupled system, τ , calculated from Eq. (3.29), with respect to the coupling strength f . The resonance frequency of the driven oscillator is set to $\omega_1 = 1.0$ and the resonance frequency of the dark mode, ω_2 , is assigned to different values. Damping rates are set to $\gamma_1 = 0.1, \gamma_2 = 0.001$. The enhancement factor is found as 18, at the coupling strengths $f = 0.019, f = 0.043, f = 0.068$, for $\omega_2 = 1.2, \omega_2 = 1.5, \omega_2 = 1.8$, respectively. As the detuning between the resonance frequencies of the oscillators is increased, a stronger coupling is required to obtain the same lifetime enhancement. The enhancement in the lifetime of the coupled system is dramatically increased when the ratio of the damping rates of the two oscillators is increased. A 2.6 fold enhancement is obtained when the ratio is 10, (see Figs 3.3 and 3.4), whereas the lifetime is enhanced 18 times when the ratio is 100. Besides, that much enhancement is obtained by weaker couplings than the ones observed in the results depicted in Fig. 3.3. The quantities are dimensionless.

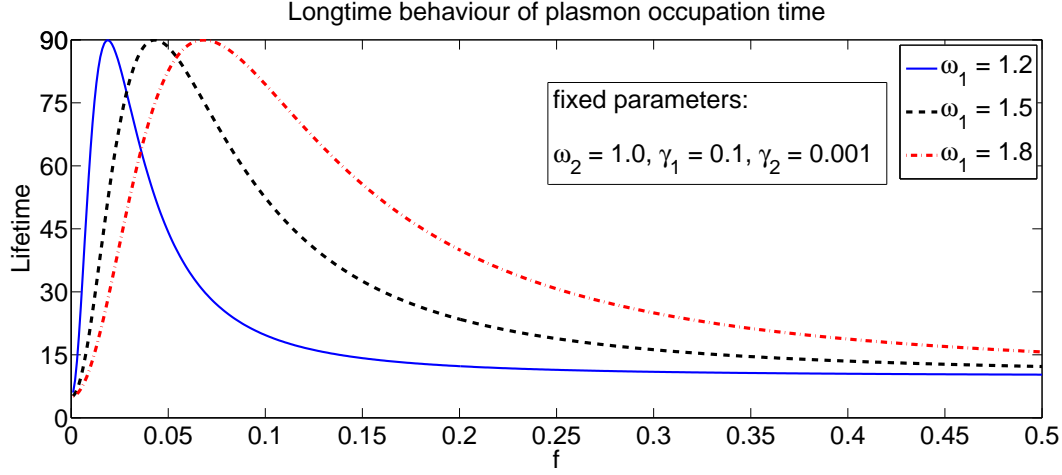


Figure 3.6: Lifetimes of the coupled system, τ , calculated from Eq. (3.29), with respect to the coupling strength f . The resonance frequency of the dark mode is set to $\omega_2 = 1.0$ and the resonance frequency of the driven oscillator, ω_1 , is assigned to different values. Damping rates are set to $\gamma_1 = 0.1, \gamma_2 = 0.001$. The enhancement factor is found as 18, at the coupling strengths $f = 0.019, f = 0.043, f = 0.068$, for $\omega_2 = 1.2, \omega_2 = 1.5, \omega_2 = 1.8$, respectively. As the detuning between the resonance frequencies of the oscillators is increased, a stronger coupling is required to obtain the same lifetime enhancement. Comparing these results with the ones shown in Fig. 3.5, a symmetry between the resonance frequencies of the oscillators is observed. The enhancement in the lifetime of the coupled system is dramatically increased when the ratio of the damping rates of the two oscillators is increased. A 2.6 fold enhancement is obtained when the ratio is 10, (see Figs 3.3 and 3.4), whereas the lifetime is enhanced 18 times when the ratio is 100. Besides, that much enhancement is obtained by weaker couplings than the ones observed in the results depicted in Fig. 3.4. The quantities are dimensionless.

Heisenberg equations are obtained by considering the case when the source is off. So in this model, it is implicitly assumed that α_1 mode is present initially, and oscillates with ω_1 before the interaction, f , is on. When the polarizations in the system decay in the absence of the source, and in the presence of coupling of the α_1 mode with the α_2 mode is of interest. When the driven particle is by itself, the system decays with the decay rate of the oscillation mode $\alpha_1^{(0)}$, that is γ_1 , given in Eq. (3.1). This is obvious, as Fig. 3.2 shows that when $f = 0$, the decay rate of the α_1 oscillations, i.e., $\Re(\lambda_1)$, is nothing but γ_1 which is assigned 0.1 in calculations. The effort is to enhance the lifetime of the oscillations on the driven particle, hence to trap the plasmon polarization for longer durations, by coupling it to an attached particle with smaller decaying rate γ_2 , utilizing path interference effects.

In the results given in Figs 3.3 and 3.4, the damping rates of the driven and the attached oscillators are assigned to $\gamma_1 = 0.1$ and $\gamma_2 = 0.01$, i.e., the ratio of the damping rates is set to 10. In this case, the maximum lifetime is found 13. This is a dimensionless scalable time value. This value corresponds to an enhancement of 2.6, as the lifetime in the absence of coupling, when $f = 0$, is 5. On the other hand, Fig. 3.5 and 3.6 shows that when the ratio of the damping rates is set to 100, i. e., $\gamma_2 = 0.001$, the enhancement dramatically increases, up to 18-fold, corresponding to a lifetime of $\tau = 90$. It is observed in Fig. 3.3 that when the ratio of the damping rates is 10, the maximum lifetime enhancement is achieved at $f = 0.066$, $f = 0.150$, $f = 0.240$ for fixed $\omega_1 = 1.0$ and $\omega_2 = 1.2$, $\omega_2 = 1.5$, $\omega_2 = 1.8$, respectively. Fig. 3.3 shows that there is symmetry between ω_1 and ω_2 . So, farther the resonance frequencies ω_1 and ω_2 , of the modes are away from each other, stronger the coupling coefficient f is required to achieve the same lifetime enhancement. This also follows from Figs 3.5 and 3.6. When the ratio of the damping rates is 100, the maximum lifetime enhancement is achieved at $f = 0.019$, $f = 0.043$, $f = 0.068$ for fixed $\omega_1 = 1.0$ and $\omega_2 = 1.2$, $\omega_2 = 1.5$, $\omega_2 = 1.8$, respectively. Comparing the cases of the two different ratio of the damping rates, one can also conclude that the maximum lifetime enhancement is achieved by weaker couplings, that is, by smaller values of f , in case where the ratio of damping rates is larger, i.e., 100 in this problem.

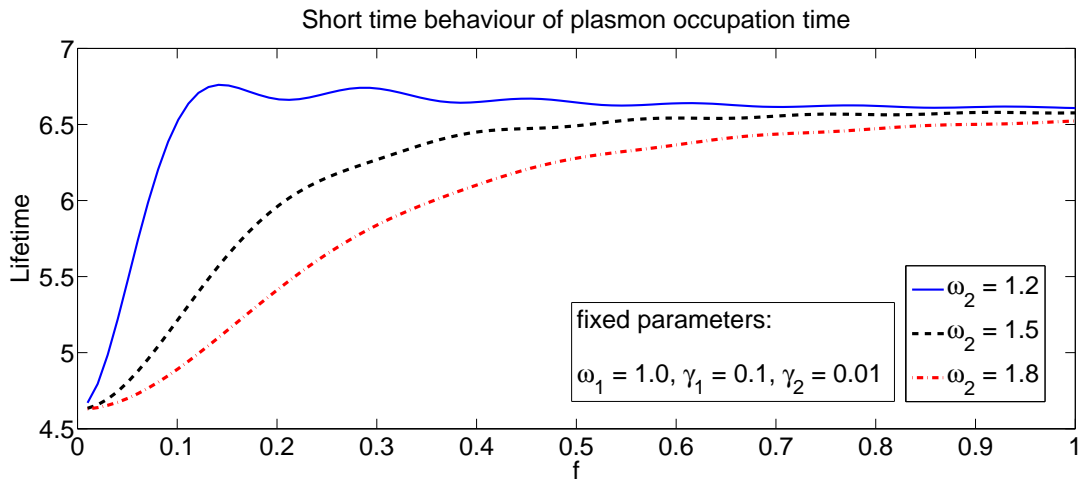


Figure 3.7: Lifetimes of the coupled system, τ , with respect to the coupling strength f , calculated by finite integration of the right hand side of Eq. (3.29) over time. The resonance frequency of the driven oscillator is set to $\omega_1 = 1.0$ and the resonance frequency of the dark mode, ω_2 , is assigned to different values. Damping rates are set to $\gamma_1 = 0.1, \gamma_2 = 0.01$. The maximum enhancement factor is found as 1.4. This value is calculated as 2.6 for the long term (by integration up to infinity, see Fig. 3.3). The quantities are dimensionless.

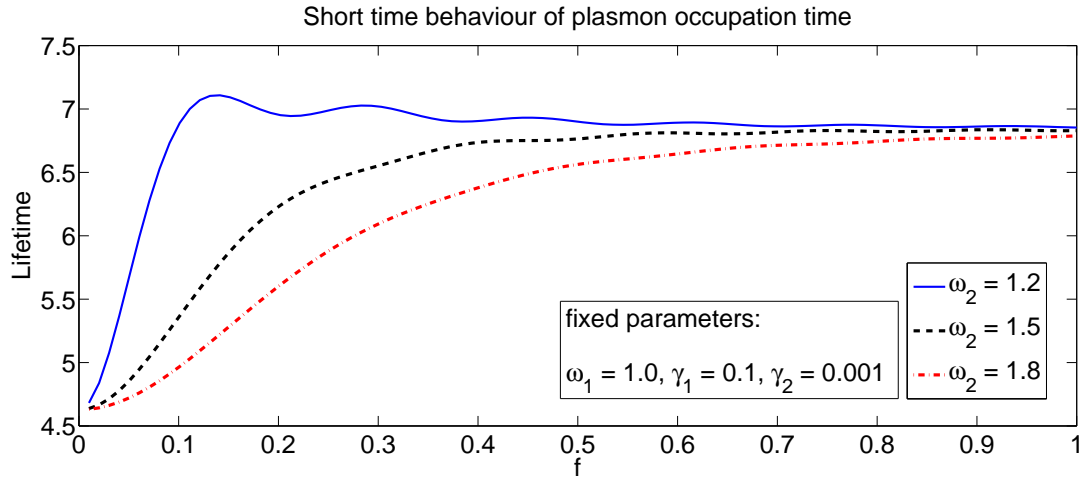


Figure 3.8: Lifetimes of the coupled system, τ , with respect to the coupling strength f , calculated by finite integration of the right hand side of Eq. (3.29) over time. The resonance frequency of the driven oscillator is set to $\omega_1 = 1.0$ and the resonance frequency of the dark mode, ω_2 , is assigned to different values. Differently from the case depicted in Fig. 3.7, damping rates are set to $\gamma_1 = 0.1, \gamma_2 = 0.001$. The maximum enhancement factor is once again found as 1.4. This value is calculated as 18 for the long term (by integration up to infinity, see Fig. 3.5). The quantities are dimensionless.

3.1.2 Short term behaviour of the plasmon decay

The results in Figs 3.3-3.6 are based on the definition of the lifetime, as in Eq. (3.29), where the total number of plasmons are integrated over time up to infinity. So these outcomes picture the long time behaviour of the plasmonic systems. This corresponds to a physical situation where a plasmonic system is illuminated by a pulse and then the polarization on the system is measured for a long time. Such trappings for prolonged durations is useful, for instance, in solar cell applications.

In order to have an understanding about the behaviour of the oscillations for shorter durations, the integrations in Eq. (3.29) are performed up to a finite time value. Fig. 3.7 shows the plasmon durations with respect to the coupling strength f , for the integrals in Eq. (3.29) carried up to $t = 20$. The same oscillation parameters with the ones used in Fig. 3.3, are used. The cases depicted by dashed and dashed-dotted curves demonstrate that the lifetime is enhanced with increasing coupling strength. The case depicted by solid curve where the resonance frequencies of the oscillators are closest, demonstrate that the lifetime is enhanced with increasing couplings at first, and then becomes almost constant. All three cases shown in Fig. 3.7 are quite different from the associated results, given in Fig. 3.3, obtained by integration over time up to infinity. For the cases of integrations up to infinity, the lifetime is suppressed for all couplings larger than a particular optimal value, as shown in Figs 3.3-3.6. Comparison of the results of the infinite and finite integrations shows that the lifetime is not extended much in the short term. It raises from 4.6 to ~ 6.5 (1.4 times) in the short time calculations. However, in the long time calculations, the lifetime is enhanced from 5 to 13, i. e., 2.6 times. This means final saturated enhancement can not be obtained at the earlier times of the coupling. This outcome is more striking in the case when the ratio of the decay rates is higher. Fig. 3.8 shows the finite integration lifetime calculations with the same resonance frequencies as the ones in Fig. 3.7, but with a different ratio of the damping rates. In this case $\gamma_1 = 0.1$ but $\gamma_2 = 0.001$. Even for the case of higher ratio of the damping rates, the finite integration results in a lifetime from about 4.6 to 6.5-7. This is very trivial compared to the case of integration up to infinity, where the lifetime is enhanced to 90.

In Fig. 3.9, blue and green curves depict how the oscillation modes on the driven and

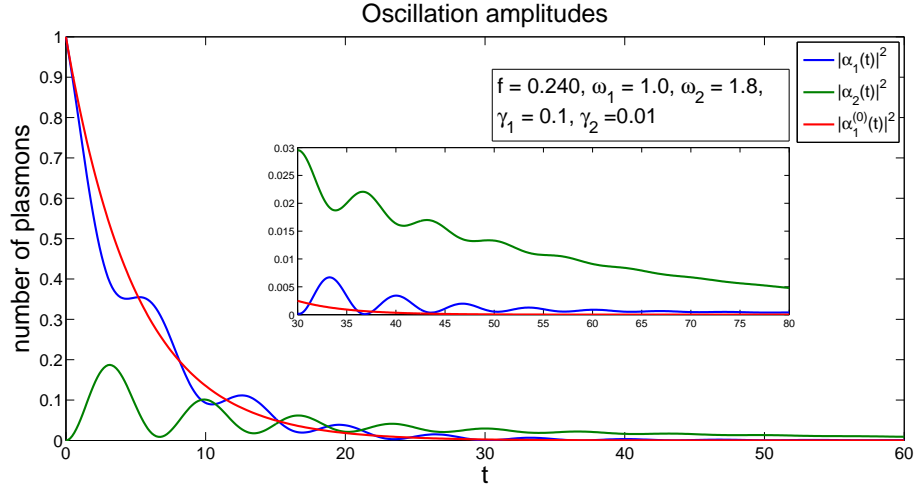


Figure 3.9: Oscillation modes $|\alpha_1|^2$ and $|\alpha_2|^2$, corresponding the number of plasmons in the polarization modes, belonging the driven (blue) and the attached (green) particles, respectively. The oscillation parameters are the same as the ones depicted by the red dashed-dotted curve in Fig. 3.3: $\omega_1 = 1.0$, $\omega_2 = 1.8$, $\gamma_1 = 0.1$, $\gamma_2 = 0.01$. The coupling coefficient f is 0.240. This is the value corresponding to the longest lifetime found in the calculation shown by the red dashed-dotted curve in Fig. 3.3. Red curve depicts the number of plasmons in the oscillations on the driven particle when the attached particle is absent. The inset graph shows the oscillations amplitudes zoomed in a later timescale, starting from 30, emphasizing that the plasmon oscillation survives for longer times essentially on the attached particle in case of coupling, shown by the green curve. The quantities are dimensionless.

the attached particles decay in time for the same parameter set as the one assigned in the case demonstrated by the the red dashed-dotted curve in Fig. 3.3. The coupling strength f is arranged to 0.240, that corresponds to the longest lifetime (found in previous calculations). The number of plasmons on the driven oscillator for the case when there is no coupling is also shown (by the red curve) in Fig. 3.9 for comparison. It is more obvious in the inset graph of Fig. 3.9 that for the case that there is no interaction between particles, the number of plasmons in the system drops zero and remains so at an earlier time, whereas the energy transfers back and forth intensely between the two modes at earliest times and then dominantly localized on the attached particle for later times, for the case of coupling.

3.2 Numerical Maxwell simulations for a 3D coupled plasmonic system

In this section, the Maxwell's equations of a three dimensional plasmonic system are numerically solved. In this treatment the plasmonic structures are examined with their true geometries, i.e., with spatial extensions. This enables to take the retardation effects into account. The decay time of electromagnetic energy on a cylindrical metal nanorod is compared with the one calculated when a smaller cylindrical metal nanorod is attached. The attached metal nanorod supports a mode with a longer lifetime than the mode supported by the first (larger) nanorod. The system is excited by a Gaussian pulse which is resonant to the larger nanorod and nonresonant to the attached nanorod. Simulations are performed with finite difference time domain (FDTD) method [53], using a free software package called MIT Electromagnetic Equation Propagation (MEEP) [54].

The computational geometry consists of two infinite cylindrical metal nanorods, with diameters 50 nm and 10 nm. They are separated by a distance of 10 nm, on the horizontal axis, as illustrated in Fig. 3.10. The problem is reduced to two dimensions due to the symmetry along the axes of the rods. The two dimensional cross section of the system is considered. The source exciting the system is a broad Gaussian pulse (with a beam width of ~ 55 fs), corresponding to a sharp peak in frequency domain. The source is located 10 nm to the left of the driven oscillator, referred as the metal nanostructure 1 (MNS1). Centres of the source, MNS1 and the attached particle, referred as the metal nanostructure 2 (MNS2), all lie on the horizontal axis.

The Lorentz-Drude model is used to describe the dielectric functions of the materials of MNS1 and MNS2 [55]. According to this model, the dielectric function of a metal is

$$\epsilon(\omega) = 1 - \frac{f_1 \omega_p^2}{\omega^2 + i\gamma_1 \omega} + \sum_{j=2}^n \frac{f_j \omega_p^2}{\omega_{0,j}^2 - \omega^2 - i\gamma_j \omega}, \quad (3.32)$$

where f is the oscillation strength, ω_p is the plasma frequency, ω_0 is the resonance frequency, and γ is the damping frequency. In Eq. (3.32), the second term is the Drude term and it refers to the intraband effects (free electron effects). The last term is the

	resonance frequency, ω_0 (eV)	plasma frequency, ω_p (eV)	damping frequency, γ (eV)	oscillation strength, f
MNS1	2.976	9.03	0.873	2
MNS2	3.738	9.01	0.055	3

Table 3.1: Lorentz parameters used in computations.

Lorentz term and it is a summation function of multiple resonance terms. These terms refer to the interband effects (bound-electron effects). In order to avoid complexities, the response of the two oscillators are arranged such that each structure has single mode in the associated spectral region, see Fig. 3.11. That is, there is only one nonzero term among the terms in the summation function. The Drude term is also set to zero. Lorentz parameters used in the computations are given in Table 3.1. The aim is to show that the lifetime of the plasmonic system is enhanced under the retardation effects as well. Hence, for proof of principle, hypothetical values are used. One can check Ref. [56] to compare the actual Lorentz parameters for bulk metals which are not much different than the ones used in these calculations.

The system considered is the following. MNS1 supports a polarization mode which can be driven by a source field. MNS2 supports a polarization mode that survives for longer durations but can hardly be driven by the source field. These conditions are provided by the scattering cross sections of each structure. The scattering cross sections of two dimensional rods, MNS1 and MNS2, with radii 50, and 10 nm, respectively, are calculated. The results are shown in Fig. 3.11. The peak frequency of the scattering cross section of MNS1 is calculated as 331.5 nm. The central frequency of the Gaussian source is arranged to coincide with this frequency in lifetime computations. The width of the Gaussian is assigned so that it does not overlap with the scattering cross section peak (resonance) of MNS2. The Gaussian distribution function of central frequency 331.5 nm and of width $1/50$ of the central frequency is also shown in Fig. 3.11. The spectral width of the plasmon mode of the driven oscillator, MNS1 is very broad compared to that of the attached oscillator, MNS2. That is, the mode supported by MNS2 has longer lifetime than that of MNS1.

The Gaussian source is sharp in the frequency domain, that is, the intensity of the

frequencies lying in the neighbourhood of the resonance of MNS2 is very small. So it can be assumed that the source hardly excites the polarization mode of MNS2. In addition, the spectral width of MNS1 covers the resonance of MNS2. In other words, the source field is arranged to drive essentially the polarization mode of MNS1, and the polarization field supported by MNS2 is induced indirectly, i.e., not by the incident field but by the polarization field excited by the plasmon field induced in MNS1.

The lifetime of the polarization supported by MNS1 is examined by calculating the decaying of the near-field energy on MNS1. This energy is obtained by the electromagnetic energy density integrated in a box surrounding MNS1, after the source leaves the medium. It is demonstrated that the lifetime of the polarization on MNS1 is enhanced by the attached MNS2, supporting a polarization mode that survives for longer durations but can hardly be driven by the source. The decay time of the total electromagnetic energy is calculated inside a particular region involving MNS1, as shown in Fig. 3.10. The lifetime is defined as the time when the energy reduces to $1/e$ of its initial value, i.e., 37 percent of its initial value. The electromagnetic energy is calculated inside a square box with a center coinciding with that of MNS1. The length of the side of the box is 6 nm larger than the diameter of the particle Au, as depicted in Fig. 3.10. The decay time of the energy is calculated for two cases: (i) when MNS1 is alone and (ii) when MNS2 is attached to MNS1, with a separation of distance 10 nm.

The energy is calculated around MNS1 inside a very small box since the field of MNS2 is avoided to be contributed to the calculations. The results of the electromagnetic energy computations are shown in Fig. 3.12. The energy is normalized to unity. The oscillation lifetime in the polarization field holding on to MNS1 is enhanced when it is coupled with a metal nanostructure supporting a mode with longer lifetime, that is excited by the induced polarization on MNS1. The electromagnetic energy around MNS1 immediately decays after the source leaves the region when it is alone, as in shown in Fig. 3.12a. The data is fitted to the single-term exponential model in MATLAB. The decay rate is calculated to be 5.957 THz in the exponential fit. This corresponds to a lifetime of 0.168 fs. In Fig. 3.12b, the enhanced oscillation duration is apparently seen. This data does not fit to the single-term exponential model, so the two-term exponential model is tried. This model is perfectly fitted to

the data obtained for the case of coupled plasmonic oscillators. The two decay rates are calculated to be 6.355 and 0.08753 THz. These correspond to the lifetimes of 0.157 fs and 11.42 fs, respectively. So, it is found that there exist two exponential components decaying with different rates in the case of coupling.

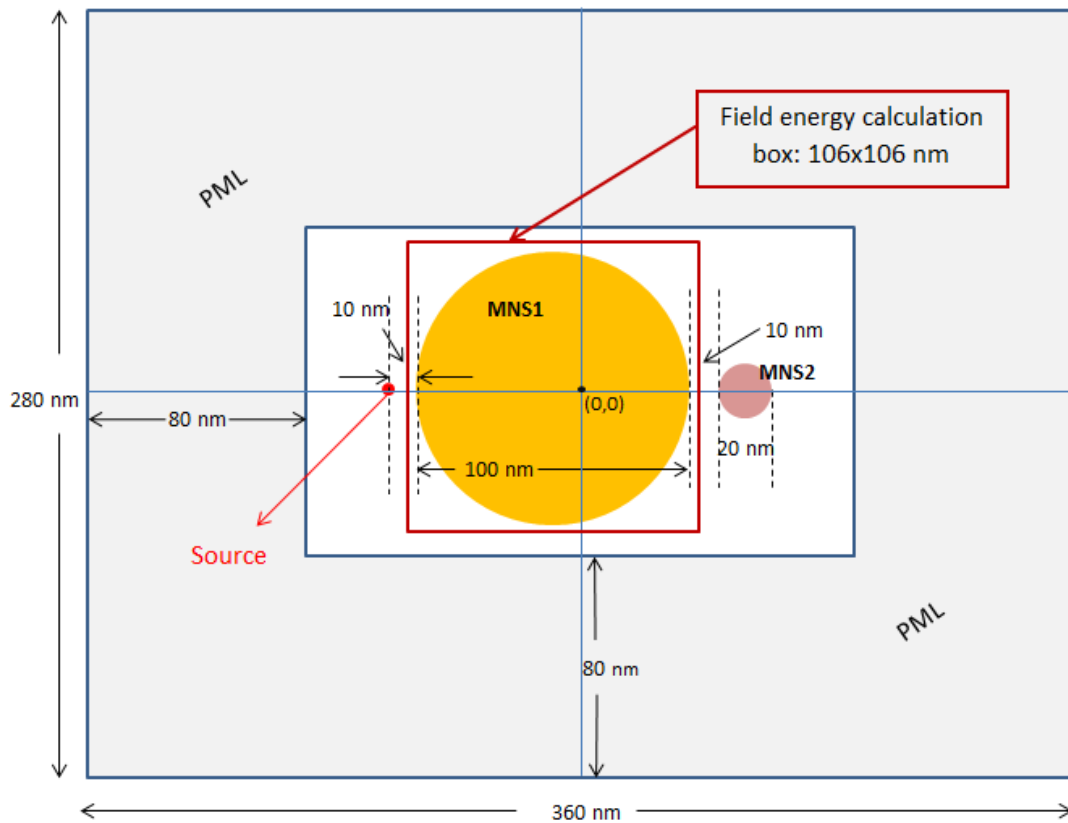


Figure 3.10: Illustration of the computational geometry. The sizes are scaled. The source is a Gaussian pulse with a narrow width in the frequency domain, resonant to MNS1. MNS1 is located 10 nm to the right of the source. Its radius is 50 nm and it is resonantly excited by the source. The radius of MNS2 is 10 nm and it is located 10 nm to the right of MNS1. The computational geometry is surrounded inside by perfectly matched layers (PMLs). A PML is an artificial absorptive layer that is commonly used to truncate computational regions with open boundaries in FDTD method. PMLs strongly absorb the electromagnetic waves from the interior of the computational geometry and there is no reflection to the interior region.

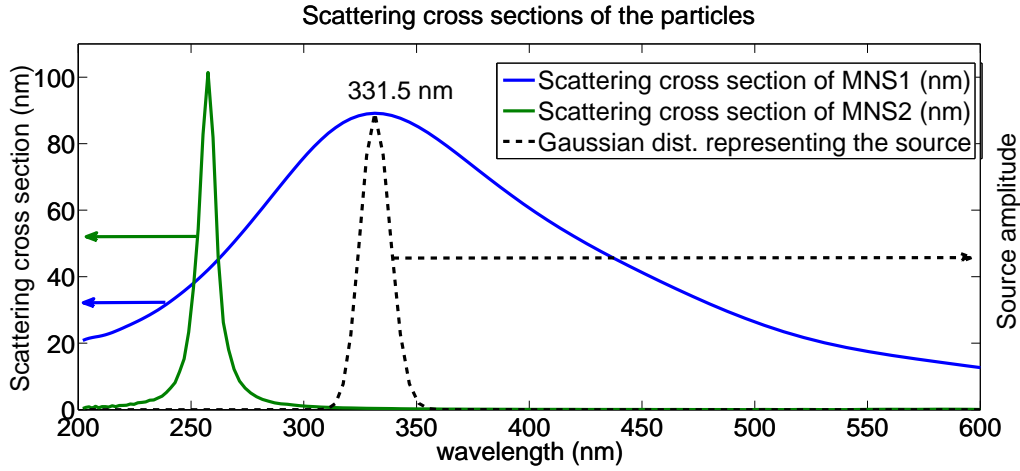


Figure 3.11: Scattering cross sections of the two structures, calculated separately in MEEP. MNS1 supports a mode with resonance frequency, $\omega_1 = 331.5$ nm, whereas MNS2 supports a mode with resonance frequency, $\omega_2 = 257.5$ nm. A Gaussian pulse with central frequency, ω_1 is shown with black dashed curve. The width of the Gaussian pulse is arranged so that it does not cover the response of MNS2. This is the Gaussian pulse emitted from the point source in Fig. 3.10. The Gaussian pulse does not overlap with the response of MNS2, but is exactly matched with the response of MNS1. The responses of the two structures overlap considerably, leading to an interaction between the two structures.

3.2.1 Short and long term behaviours of the energy

Comparing parts (a) and (b) in Fig. 3.12, more or less the same rapid decaying is observed at the first femtosecond in both calculations. The decay rates are calculated to be 5.957 THz and 6.355 THz, corresponding to the lifetimes of 0.168 fs and 0.157 fs for the uncoupled and coupled cases, respectively. The energy of the coupled case is determined by a two-term exponential function. So the energy decay of the coupled system is governed by two different rates, one of which is ~ 70 times larger than the other. The exponential term with larger decay rate has an amplitude, ~ 30 times larger than the other one. The energy of the coupled system decays very rapidly at first, i. e., the decay is governed by the higher rate. However, as apparently seen in Fig. 3.12b, the energy is almost constant after the rapid drop to ~ 10 percent of its initial value. Comparing this with the other system where MNS1 is alone, the polarization lasts for a ~ 70 times longer duration.

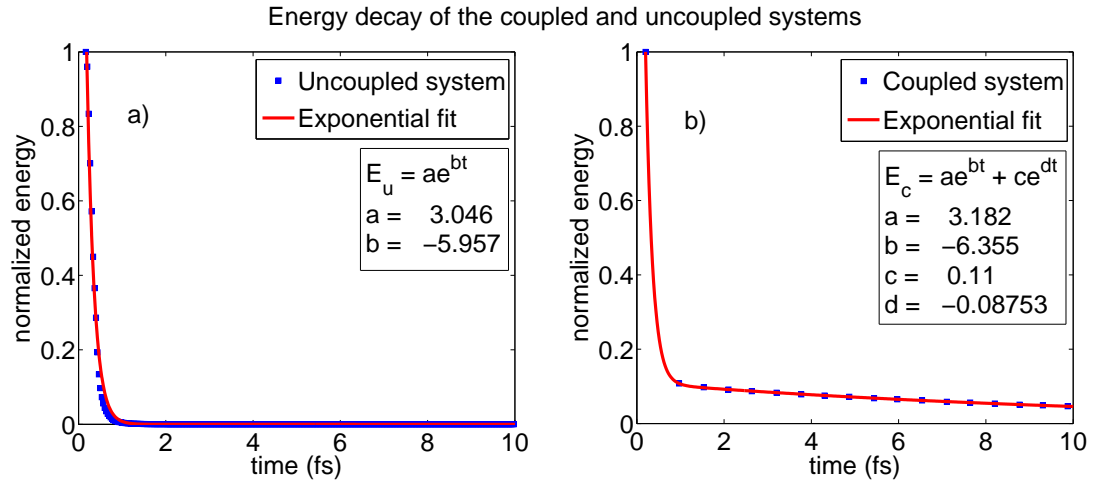


Figure 3.12: Normalized energy vs. time results for coupled and uncoupled systems. When MNS1 is alone, the electromagnetic energy around MNS1 decays rapidly (a). Longer durations are apparently observed in part (b). This is the case when MNS2 is attached to MNS1. Energy in case (b) is again calculated around MNS1. The lifetime of the oscillations on MNS1 is extended when MNS2 is attached. The exponential decay fit functions are also shown. According to the exponential parameters, when MNS2 is attached to MNS1, the electromagnetic energy around MNS1 decays with the same rate as the case when MNS1 is alone at the beginning. But for later durations, the second exponential term governs the decay. It is calculated to be 0.08753 THz, that corresponds to a ~ 70 times longer duration of the oscillations around MNS1.

3.2.2 Hybridization in the scattering cross section

Fig. 3.13 shows that the MNS1-MNS2 system is hybridized, serving as a proof of interparticle interaction. The blue and the green dashed curves stand for the scattering cross sections of MNS1 and MNS2, respectively, calculated separately. The red solid curve stands for the scattering cross section of the system where the structures are brought together. It is noted that the peak of MNS2 is shifted to smaller wavelengths. If this was a superposition rather than a hybridization, the shift would be expected to be to longer wavelengths where the amplitude of MNS1 is larger. The peak of MNS1 is shifted as well. To make sure, comparison of the cases of superposed and coupled results is presented in Fig. 3.14. It is apparently seen that the peaks are shifted in the coupled case, confirming that there is a hybridization between modes. It is a weak

hybridization since both superposed and coupled response curves are similar in shape. An apparent broadening in the response of MNS2 is observed, which predicts that the lifetime of MNS2 shortens. Although it is not as much obvious as the broadening of the peak of MNS2, it is observed that the peak of MNS1 is sharpened. This confirms the extension in the lifetime of the oscillations around MNS1 when MNS2 is attached. The Lorentz decay rates used in the computations are given in Table 3.1. It is noted that the decay rate of MNS2 is 1/16 times smaller than that of MNS1.

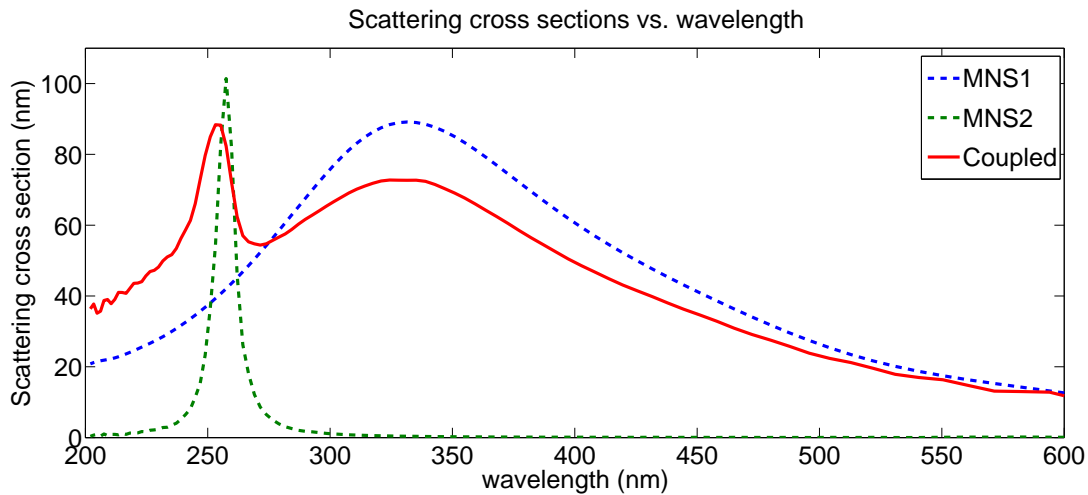


Figure 3.13: Comparison of scattering cross sections. Blue dashed curve stands for the scattering cross section of MNS1, when it is alone. Green dashed curve stands for that of MNS2, when it is alone. Red solid curve stands for the scattering cross section when the two structures interact. The scattering cross section for the coupled system displays a broadening at the resonance of MNS2 and a sharpening at the resonance of MNS1, with a shift to the left. The weak hybridization can be witnessed by these broadening and sharpening, and the shift of the peaks to the left, unlike a superposition depicted in Fig. 3.14.

3.3 Summary and Discussion

In this chapter, the linear response of a coupled plasmonic system is investigated. It is examined that how coupling of two plasmonic structures affects the lifetime of the plasmonic modes. One of the structures supports a plasmon mode which couples to the incident radiation field. The second particle has a dark state which cannot be

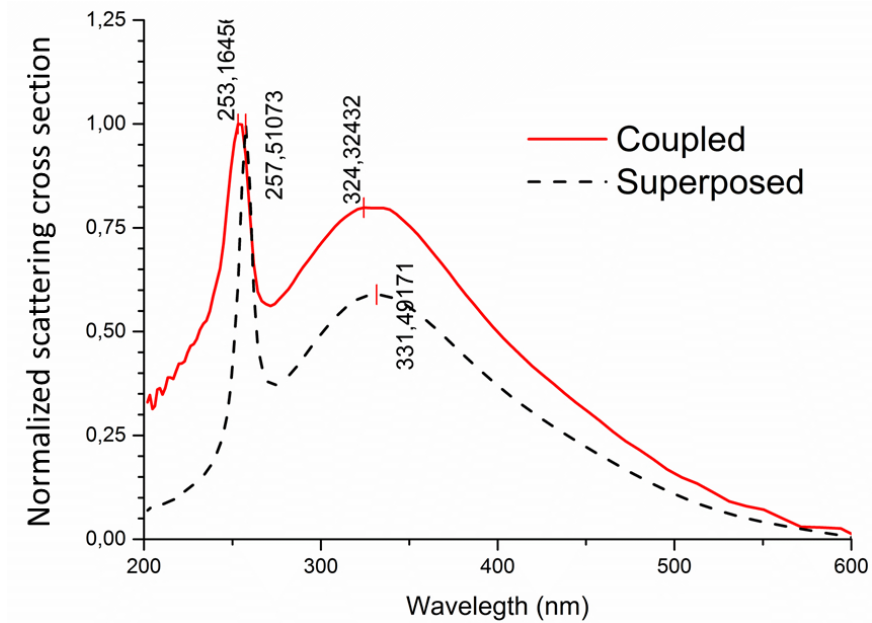


Figure 3.14: Comparison of the cases of superposition and coupling of the modes. Red curve is the normalized Lorentzian fit to the red curve in Fig. 3.13. It is the scattering cross section of the geometry where MNS1 and MNS2 are brought together and are electromagnetically coupled. Black dashed curve is obtained by adding up the blue and green dashed curves of Fig. 3.13, and fitting it to a normalized Lorentzian function. These blue and green dashed curves are the scattering cross sections of MNS1 and MNS2, calculated separately. So black dashed curve is the superposition of the responses. It is apparently seen that the peaks are shifted in the coupled case, confirming that there is a hybridization between modes. It is a weak hybridization since both superposed and coupled response curves are similar in shape.

excited by incident radiation due to the vanishing overlap integral (Eq. (3.1)). It can be excited by the induced polarization field on the driven structure.

In section 3.1, the decaying of the oscillators are studied in the case where the first mode is initially excited. The polarization modes are treated as quantum harmonic oscillators and an eigenvalue equation is obtained by deriving coupled equations of motions from the Heisenberg equation. Since entanglement-like properties are out of interest, the quantum operators are changed with their expectation value parameters, that are the amplitudes of the plasmons as a function of time. Eigenvalue equation is lack of a driving force since the decaying properties are explored. The lifetime of the coupled plasmonic system is defined by Eq. (3.29), by which the long term behaviour is studied. The lifetime is calculated for couple of sets of oscillation parameters ($\omega_{1,2}, \gamma_{1,2}$, corresponding to the resonances and damping rates of the two plasmonic oscillators in the coupled system) with respect to the coupling strength parameter, f . The results presented in Fig.s 3.3-3.6 show that the lifetime of the polarizations, which is defined by the total number of surviving plasmons in the coupled system, is enhanced by factors of 2.6 and 18 for the cases of the ratios of the damping rates of 10 and 100, respectively. For changing values of the resonances of the oscillators, ω_1 and ω_2 , the results show that there is a symmetry, i.e., $\omega_{1,2} = \omega_{2,1}$. This expected because the eigenvalue equation becomes symmetric when the source term is removed. Additionally, farther the spectral positions of the modes ω_1 and ω_2 , are away from each other, stronger the coupling coefficient, f , is required to achieve the same lifetime enhancement, as one should expect. Comparing the cases of two different ratios of the damping rates, one can also conclude that the maximum lifetime enhancement is achieved by weaker couplings, that is, by smaller values of f , in case where the ratio of damping rates is higher, i.e., 100 in this problem. Specifically, the highest enhancement is achieved by the coupling coefficients, $f = 0.019, f = 0.043, f = 0.068$ for different values of the resonance frequencies in the case of higher ratio of the damping rates, as shown in Fig.s 3.5 and 3.6. However, in the cases of lower ratio of the damping rates, the highest enhancement is achieved at $f = 0.066, f = 0.150, f = 0.240$, as shown in Fig.s 3.3 and 3.4.

The short time behaviour of the coupled system is examined as well. The expressions in Eq. (3.29) are evaluated up to a finite time value instead of infinity. The limit

of the finite integration is set to 20, in units of inverse frequency, where the unit of frequency is 1. One can compare this value with the time scale of the oscillation amplitudes in Fig. 3.9. In the case of infinite integration, the lifetime enhancement increases up to a particular f , and decreases afterwards. In the short term behaviour, lifetime increases up to a smaller value and then is constant with increasing f . One may conclude from the comparison of finite and infinite integration calculations that the number of plasmons continue to count up for later times. The inset graph of Fig. 3.9 shows that α_2 oscillations last for a long time; it seems the energy is transferred back and forth between the modes at first, then, it is saturated to a very small value, and slowly decaying pattern, engaged on the attached (longer lifetime) particle. This pattern seems to make a big difference in case where the ratio of the damping rates are large.

It is demonstrated that the oscillation lifetime of a coupled system is enhanced via excitement of a high-quality oscillator by the induced polarization of a low-quality oscillator. This is guaranteed by assigning zero to the initial value of high-quality oscillation amplitude. So, it reads, in the time evolution of the system, the the short lifetime polarization, that is initially present, excites the long lifetime polarization and due to the interference of the paths induced by the weak hybridization, energy transfer from short lifetime to long lifetime mode results in enhancement in the lifetime of the coupled system.

This outcome, obtained in section 3.1, is confirmed by Maxwell simulations of a similar model system with physical structures (structures having spatial extensions) in three dimensions in section 3.2. In this way, the retardation effects are taken into consideration. Two metal nanoparticles with different sizes, hence with different resonances are considered. The dielectric parameters of the metal structures are introduced by Lorentz dielectric function [55], with the hypothetical (but physical) parameters given in Table 3.1.

In section 3.2, lifetime of an oscillation is described by the decay time of the total electromagnetic energy computed inside a box surrounding the structure which supports the associated oscillation mode. Computations are performed using FDTD by MEEP. It is demonstrated that the lifetime of a metal nanostructure, which is referred

as MNS1, is enhanced by an attached oscillator, MNS2, which has a longer lifetime. Scattering cross sections of the systems where (i) MNS1 is alone, where (ii) MNS2 is alone, and where (iii) both structures are brought together are computed in MEEP. Sizes, shapes and dielectric functions of the structures are tuned such that each supports only one resonance mode. Thus, coupling of two particular modes is explored and complexities that may arise from couplings to other resonance modes are avoided. Two modes shown in Fig. 3.11 are arranged by assigning appropriate Lorentz parameters, so that the mode supported by MNS2 is sharp and the mode supported by MNS1 is broad and covers the response of MNS2. The Gaussian source used in the energy calculations is determined according to the spectral position of the scattering cross section of MNS1. MNS1 is the one with short lifetime and is excited by the incident field. MNS2 is the attached structure with a longer lifetime, and assumed to be unable to be excited by the incident field. In the simulation, this is provided by a large detuning to the Gaussian source. The width of the Gaussian pulse is determined so that it does not excite MNS2, i.e. does not overlap with the response of MNS2. The central frequency of the Gaussian source is tuned resonant to the response peak of MNS1.

The results of the energy calculations are shown in Fig. 3.12. Normalized energy is computed for coupled and uncoupled cases with respect to time. Comparing these cases shown in parts (a) and (b) in Fig. 3.12, it is observed that the energy decays very rapidly, with more or less the same decay rate at the first femtosecond, in both calculations. The decay rate at the first femtosecond in both cases are calculated to be ~ 6 THz. This is the decay rate of the uncoupled case along the whole timescale. The energy of the coupled case is determined by a two-term exponential function. So the energy decay of the coupled system is governed by two different rates, one of which is ~ 70 times larger than the other. Besides, the exponential term with larger decay rate has an amplitude which is ~ 30 times larger than that of the other. The energy of the coupled system decays very rapidly at the beginning, i. e., the decay is governed by the higher rate. However, as apparently seen in Fig. 3.12b, the energy is almost constant after the rapid drop to ~ 10 percent of its initial value. Comparing this with the uncoupled system where MNS1 is alone, the polarization lasts for a ~ 70 times longer duration. This is a remarkable result, as can be utilized to enhance the light harvesting efficiency in photovoltaic devices.

Fano resonances enable the absorbed energy rate to be governed by the decaying properties of the long lifetime oscillator in a coupled system of two plasmonic oscillators, where the system is excited by driving the the short-lifetime oscillator. The results of sections 3.1 and 3.2 can be evaluated by comparing Figs. 3.9 with Fig. 3.12. Both results show that in the long term, the plasmons survive obeying a lower decay rate, as a result of interaction between (attached) dark and (driven) bright modes.

In Fig. 3.11, it is shown that the MNS1-MNS2 system is hybridized. This is served as a proof of interparticle interaction. The observation of the shift of the response peak of MNS2, to smaller wavelengths proves the weak hybridization. If it was a superposition rather than a hybridization, the shift would be expected to be to longer wavelengths, where the response of MNS1 is larger. An apparent broadening in the response of MNS2 predicts that the lifetime of MNS2 shortens. The peak of MNS1 is shifted as well. Although it is not as much obvious as the broadening of the peak of MNS2, it is observed that the peak of MNS1 is sharpened. This confirms the extension in the lifetime of the oscillations around MNS1 when MNS2 is attached. Such a sharpening in the response of a Gold nanoparticle is experimentally demonstrated by Noginov et. al. 2009, as a result of coupling the plasmonic structure to a quantum emitter [12]. Sobhani et. al. 2015, demonstrates a similar band narrowing in the spectral response of an Aluminium nanoparticle as a result of coupling to an Aluminium film substrate [57]. They experimentally observe this phenomenon and demonstrate theoretically by a model based on multipolar expansion.

CHAPTER 4

SECOND HARMONIC GENERATION ENHANCEMENT IN COUPLED PLASMONIC SYSTEMS

Plasmon oscillations in metal nanostructures (MNSs) concentrate the incident light into nanometre dimensions yielding strong enhancement in the near-field intensities [2]. The localized strong polarization field leads to appearance of optical nonlinearities [8] such as enhanced Raman scattering [22], four wave mixing [23,24], two photon absorption [25–27], and second harmonic generation (SHG) [28–33]. When a quantum dot is placed on a hotspot of a plasmonic system, localized surface plasmons interact strongly with the attached quantum dot. The interaction introduces two absorption/emission paths both lying in the plasmon spectral width [34], hence making them unresolvable. The two paths operate out of phase—the first one absorbing while the second one emitting—and result in a dip in the absorption spectrum, where instead an absorption peak would be observed. Such transparencies in the plasmonic response are referred as Fano resonances [14]. This path interference phenomenon is responsible for increased fluorescence of molecules [58] and increased lifetime of plasmonic oscillations [15] which makes coherent plasmon emission possible [2, 12]. Quantum coherence effects can be used to increase the sensitivity of nanolasers with ultrafast response [59] and can enhance amplification [60, 61].

Presence of nonlinear responses can be both advantageous and disadvantageous depending on the operation of the optical device. For instance, enhanced nonlinear plasmonic conversion can be utilized in Raman imaging [62, 63], optical switching [64], etc. In particular, SHG enhancement can be useful in efficiency improvement of photovoltaic devices [65], coherence time enhancement [15, 66, 67], or generation of

entangled photon pairs [68]. On the other hand, nonlinear processes can cause losses in the signal in fiber optic cables [69], or decrease the quality factor of microwave cavities [70]. So nonlinear effects may desired to be avoided as well.

Fano resonances in the nonlinear response, with quantum objects attached on nanoparticles, can be utilized to enhance [28] and suppress [20] SHG process in plasmonic systems. The underlying mechanism relies on the cancellation of nonresonant frequency terms (in the denominator of the expression of the response) which degrade the frequency conversion by hybridized paths [20]. Fano resonances can also take place in two coupled classical plasmonic oscillators [34, 35], without the existence of a quantum nature. It is experimentally demonstrated that coupling with dark modes (which have longer lifetimes) [36–38] can result in Fano resonances.

In this chapter, in section 4.1, a theoretical model examining the second harmonic (SH) response of a coupled plasmonic system consisting of two MNSs, is presented. It is demonstrated that SHG can be adjusted by tuning the coupling between the two plasmonic oscillators. This phenomenon is examined by assigning different values to the oscillation parameters, namely, the coupling strengths f_1 and f_2 , and the damping frequency of the long lifetime nanostructure, γ_b . The optimum parameter sets are reported both for enhancement and suppression phenomena.

In section 4.2, an experimental study on the SH response of a plasmonic system consisting of silver nanowires (AgNWs) and silver bipyramid nanoparticles (AgNPs) is presented. The bipyramid shape provides long-lived dark states, and the excitation of the AgNWs interacts with this sharp mode. The sample composed of an AgNP of ~ 100 nm size and an AgNW of ~ 60 nm diameter and several microns length, placed on a dielectric (glass) surface. When a 1064 nm near-infrared excitation laser is focused solely on an isolated AgNW, a weak 532 nm SHG signal is observed. On the contrary, when the coupled system is excited in the vicinity of the coupling region, the observed SH signal increases up to 30-fold. This enhancement is demonstrated by performing an *in situ* experiment, where the laser focus is moved along the AgNW axis. It is observed that the generated SH signal increases by a factor of 30, when the focus passes through the AgNP coupled region. The SHG level at AgNW body that is a few μm away from the AgNP is at the same level as that of an isolated AgNW.

The SH signal from a bare AgNP is found to be only 1/6 of the isolated AgNW. The observed enhancement can be obtained in the theoretical model by coupling the converter with a MNS which has a 10 times longer plasmon lifetime with particular coupling strengths among modes.

4.1 Theoretical model examining second harmonic response in coupled plasmonic systems

A theoretical model examining the second harmonic (SH) response of a coupled plasmonic system consisting of two metal nanostructures (MNSs) is developed. The first MNS supports two plasmon modes with frequencies (ω_1, ω_2) resonant to the incident linear (ω) and the second harmonic (2ω) frequencies, see Fig. 4.1. This is the oscillator driven in the ω_1 mode and is a SH converter. A second nanostructure, which supports single plasmon mode with a narrower response in the frequency domain, is attached to the driven oscillator. This mode cannot be excited by the incident field, since it is a dark state. The natural frequency (ω_b) of the attached oscillator is in between the spectral positions of the two modes supported by the SH converter, ω_1 and ω_2 . So, the attached oscillator can couple to both modes of the driven oscillator.

Coupled differential equations governing the dynamics of the system, and the time evolutions of these equations are obtained. In this simple approach, the polarization modes of the MNSs are treated as harmonic oscillators excited either by incident classical field (ω) or by the induced polarization fields. The dark state is excited indirectly by coupling to the plasmon modes, ω_1 and ω_2 , in which ω and 2ω oscillations emerge. Hamiltonian of the system is obtained and the Heisenberg equation for each oscillation mode is derived. Since entanglement-like features are out of interest, only the amplitudes of the oscillations are examined. The second harmonic response is defined by the total number of SH plasmons in the system.

The MNSs are treated as if they do not have spatial extensions, i.e. they are point particles. In the physical situation, however, the particles must have sizes and hence there must be retardation effects. In ref. [20], coupling of a MNS and a quantum emitter object is treated with a similar theoretical (oscillator) model. It is shown that this sim-

ple model can predict the amount and the spectral position of the SHG enhancement. This is done by comparing the results with the 3D simulations performed by using MNPBEM Toolbox in MATLAB [71]. The simulations take the retardation effects into account, that is, the physical objects are simulated with their true geometries.

The ω_1 mode (see Fig. 4.1) of the converter nanostructure is driven by a monochromatic wave of frequency ω . The localized plasmons, oscillating with frequency ω , combine to yield 2ω plasmons, emerging in the ω_2 mode. The auxiliary MNS (supporting long-lived dark state) interacts with the two modes. The aim is to observe the effects of coupling of the dark state to the ω_1 and ω_2 plasmon modes, that is Fano resonance. So, the number of 2ω plasmons are calculated for two cases. That is, (i) when the driven SH generator metal nanostructure (MNS) is by itself and (ii) when the second MNS is attached to system.

The treatment is different than the one in Ref. [20] in the following manner. In Ref. [20], the attached auxiliary particle is a quantum emitter: The linewidth of the quantum emitter is quite sharp, so couples only to ω_2 mode. Here the linewidth of the auxiliary particle is relatively large because it is a plasmonic oscillator. So, coupling of the dark mode to both modes of the SH converter is considered. Therefore there exist 2ω plasmon oscillations in all three modes. The total number of these plasmons are calculated in order to include the contributions from all modes.

The total number of SH plasmons can be tuned due to Fano resonance by adjusting the couplings between two MNSs. So, by carefully choosing the system parameters, one can maximize the SH response of this system. Fano coupling effects arise when the interacting particles have different decaying rates. A particle with small decaying rate is regarded as a high quality oscillator. Because it can support polarization oscillations for longer durations compared to the low quality particles with large decaying rates. Different decaying properties lead to path interference effects called Fano resonance and make the SH response tunable in coupled systems.

The resonance frequencies of the driven oscillator are ω_1 and ω_2 . These are around the frequencies of the incident linear (ω) and the SH (2ω) fields, respectively. The MNS supporting single plasmon polariton mode (ω_b) with smaller decay rate is attached to the converter. The plasmon polarization mode of the auxiliary particle, with frequency

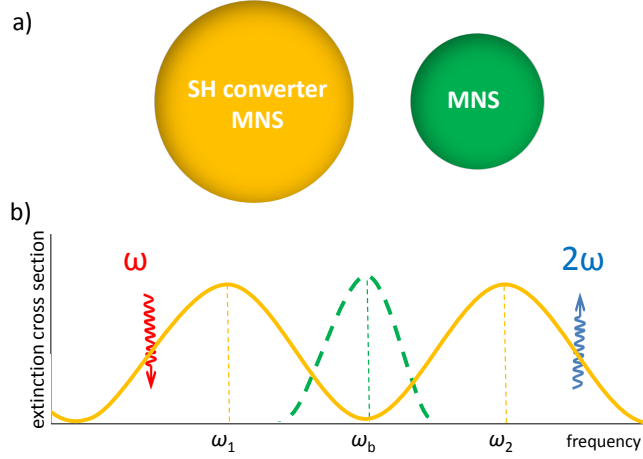


Figure 4.1: A representative picture (a) of the coupled oscillators, and their resonances (b). The driven oscillator (SH converter) supports two modes, ω_1 and ω_2 , where the two frequencies are around the driving and SH field frequencies, respectively. The attached oscillator, which has a longer lifetime, is coupled with the driven oscillator introducing path interference effects in the SH response.

ω_b , cannot be driven by the incident field. It is both off-resonant to the drive and is a dark state which cannot be coupled to the far-field. The coupling integral,

$$\varepsilon_b \propto \int E_b^*(\mathbf{r}) E_{exc}(\mathbf{r}) d^3 \mathbf{r},$$

vanishes due to parity arguments, where E_b , and E_{exc} are the electric fields of the dark mode and the excitation.

The system is illustrated in Fig. (4.1). An incident pump field oscillating with a frequency ω drives the SH converter structure and induces the ω_1 plasmon polariton field. This is the linear polarization field. The incident pump field is confined to nanoscale dimension in ω_1 plasmon polariton mode. This is a very strong field with very high density of plasmons, enabling nonlinear processes. Second harmonic generation (SHG) process emerges into the second mode, ω_2 , supported by the driven oscillator. Two of the ω plasmons in the ω_1 mode annihilate and one 2ω plasmon is created instead [72]. When the structure with smaller decay rate is attached to the system, linear and SH polarization fields interact with the mode of this structure of resonance frequency ω_b . By adjusting the system parameters, the path interference

effects are tuned and it is managed to achieve frequency conversion from linear to SH polarization, leading to an enhancement in the number of 2ω plasmons. On the contrary, these interactions can be arranged to suppress the generation of 2ω plasmons.

The enhancement and suppression phenomena can be explained using the arguments in Ref. [20]. The terms corresponding to the absorption paths explicitly appear on the expression representing SH amplitude in the mentioned reference. This expression is analytically derived. The mode on the attached structure is coupled to both modes in the model examined in this study, leading the 2ω plasmons to appear in all modes. Therefore deriving such an expression representing the second harmonic amplitude analytically is not possible. However, the mechanism is similar. By arranging the terms in the denominator of this expression (Eq. (9) in Ref. [20]) so that they cancel out, a blow up of the amplitude can be provided, leading to SHG enhancement, for appropriate coupling parameters. A similar manipulation can be done to obtain SHG suppression as well.

Hamiltonian of the system is written as the sum of the following components,

$$\hat{H}_a = \hbar\omega_1\hat{a}_1^\dagger\hat{a}_1 + \hbar\omega_2\hat{a}_2^\dagger\hat{a}_2, \quad (4.1)$$

$$\hat{H}_b = \hbar\omega_b\hat{b}^\dagger\hat{b}, \quad (4.2)$$

$$\hat{H}_{int} = \hbar(f_1\hat{a}_1^\dagger\hat{b} + f_1^*\hat{a}_1\hat{b}^\dagger) + \hbar(f_2\hat{a}_2^\dagger\hat{b} + f_2^*\hat{a}_2\hat{b}^\dagger), \quad (4.3)$$

$$\hat{H}_p = i\hbar(\hat{a}_1^\dagger\varepsilon_p e^{-i\omega t} - \hat{a}_1\varepsilon_p^* e^{i\omega t}), \quad (4.4)$$

$$\hat{H}_{sh} = \hbar\chi^{(2)}(\hat{a}_2^\dagger\hat{a}_1\hat{a}_1 + \hat{a}_1^\dagger\hat{a}_1^\dagger\hat{a}_2). \quad (4.5)$$

\hat{H}_a and \hat{H}_b given in Eq.s (4.1) and (4.2) are the energy operators of plasmon polariton excitations in the system. \hat{H}_a is the energy of the driven SH converter supporting two modes with frequencies ω_1 and ω_2 . \hat{H}_b is the energy of the attached oscillator supporting single mode with frequency ω_b . \hat{a}_1 , \hat{a}_2 , and \hat{b} are the annihilation operators for the collective plasmon oscillations in the driven and the attached MNSs, respectively. These will soon represent the amplitudes of the associated oscillations.

\hat{H}_{int} given in Eq. (4.3), is the interaction energy among the plasmon polariton fields,

f_1 and f_2 being the coupling matrix elements

$$f_{1,2} \propto \int E_b^*(\mathbf{r}) E_{1,2}(\mathbf{r}) d^3\mathbf{r},$$

determining the strengths of the couplings. The plasmon mode supported by the attached nanostructure is coupled both with the linear and the SH polarized modes supported by the driven SH converter via the coupling coefficients f_1 and f_2 , respectively. $f_{1,2}$ are in units of frequency.

\hat{H}_p given in Eq. (4.4) is the energy supplied by the incident field. Since the incident field drives the \hat{a}_1 mode, only this operator appears in the expression.

Finally, \hat{H}_{sh} , given in Eq. (4.5), is the energy term governing the SHG process. In Eq. (4.5), two low energetic plasmons in \hat{a}_1 mode oscillating at ω , combine to generate a SH plasmon in \hat{a}_2 mode, oscillating at 2ω . The parameter $\chi^{(2)}$, in units of frequency, is proportional to the SH susceptibility

$$\chi^{(2)} \propto \int E_2^*(\mathbf{r}) E_1^2(\mathbf{r}) d^3\mathbf{r},$$

of the oscillator.

So, the total Hamiltonian of the system is

$$\hat{H} = \hat{H}_a + \hat{H}_b + \hat{H}_{int} + \hat{H}_p + \hat{H}_{sh}. \quad (4.6)$$

Equations of motions are derived by using the Heisenberg equation. In Heisenberg picture, any observable \hat{A} evaluates in time obeying $i\hbar\dot{\hat{A}} = [\hat{A}, \hat{H}]$. There are three operators of interest, \hat{a}_1 , \hat{a}_2 , and \hat{b} , for three plasmon oscillaton modes in the system. The dynamics of these operators is obtained

$$\dot{\hat{a}}_1 = -i\omega_1\hat{a}_1 - f_1\hat{b} + \epsilon_p e^{-i\omega t} - 2i\chi^{(2)}\hat{a}_1^\dagger\hat{a}_2, \quad (4.7)$$

$$\dot{\hat{a}}_2 = -i\omega_2\hat{a}_2 - f_2\hat{b} + i\chi^{(2)}\hat{a}_1\hat{a}_1, \quad (4.8)$$

$$\dot{\hat{b}} = -i\omega_b\hat{b} - f_1^*\hat{a}_1 - if_2^*\hat{a}_2. \quad (4.9)$$

The quantum optical properties of the system, such as entanglement, are out of interest. So the quantum operators, \hat{a}_1 , \hat{a}_2 , and \hat{b} are replaced with the expectations values, α_1 , α_2 , and α_b . These expectation values are the amplitudes of the plasmon oscillations. Damping force on the structures is not included in the Hamiltonian, so the damping rates γ_1 , γ_2 and γ_b are plugged in the equations. The coupling coefficients f_1 and f_2 are assumed real to decrease the degree of complexity of the problem. Consequently, equations of motions of the plasmon amplitudes are found as

$$\dot{\alpha}_1 = (-i\omega_1 - \gamma_1)\alpha_1 - f_1\alpha_b + \epsilon_p e^{-i\omega t} - 2i\chi^{(2)}\alpha_1^*\alpha_2, \quad (4.10)$$

$$\dot{\alpha}_2 = (-i\omega_2 - \gamma_2)\alpha_2 - f_2\alpha_b + i\chi^{(2)}\alpha_1^2, \quad (4.11)$$

$$\dot{\alpha}_b = (-i\omega_b - \gamma_b)\alpha_b - f_1\alpha_1 - if_2\alpha_2, \quad (4.12)$$

where the damping rates are included.

Three coupled differential equations given in Eq.s (4.10-4.12) determines the dynamics of the plasmon fields. In the steady state, the plasmon fields can be expressed as the sum of two dominant terms with two distinct frequencies. Since the oscillation modes support the driving frequency, ω , and the second harmonic generated frequency, 2ω , the plasmon files are expressed as

$$\alpha_1(t) = \alpha_1^{(1)} e^{-i\omega t} + \alpha_1^{(2)} e^{-i2\omega t}, \quad (4.13)$$

$$\alpha_2(t) = \alpha_2^{(1)} e^{-i\omega t} + \alpha_2^{(2)} e^{-i2\omega t}, \quad (4.14)$$

$$\alpha_b(t) = \alpha_b^{(1)} e^{-i\omega t} + \alpha_b^{(2)} e^{-i2\omega t}. \quad (4.15)$$

Amplitudes $\alpha_1^{(1)}$, $\alpha_2^{(1)}$ and $\alpha_b^{(1)}$ are the amplitudes of linear plasmon oscillations oscillating with frequency ω , and $\alpha_1^{(2)}$, $\alpha_2^{(2)}$ and $\alpha_b^{(2)}$ are the amplitudes of the SH plasmon oscillations oscillating with 2ω , in the three plasmon modes.

The equations (4.10-4.12) are numerically evolved in time and then the time behaviour after steady state has been reached, is obtained. The steady state amplitudes $\alpha_1^{(2)}$, $\alpha_2^{(2)}$ and $\alpha_b^{(2)}$, exhibiting the amplitudes of SH oscillations, are determined by using the Fourier transform technique. The number of SH plasmons can be determined

by summing over the plasmons generated in all three modes as

$$N_{sh} \equiv |\alpha_1^{(2)}|^2 + |\alpha_2^{(2)}|^2 + |\alpha_b^{(2)}|^2. \quad (4.16)$$

It is noted that $e^{-i2\omega t}$ oscillations in α_1 and α_b modes are not generated in these modes. They are rather transferred from α_2 mode to α_b mode first, and then from α_b mode to α_1 mode.

In a realistic physical situation, adjusting the oscillation parameters of the driven structure (SH converter) is not practical since ω_1 and ω_2 cannot be tuned independently and it is hard to tune a manufactured material. So, tunable parameters should be the parameters belonging to the attached (auxiliary) structure. Therefore, the enhancement in the SHG for different attached plasmonic oscillators of different natural frequencies are calculated, when the remaining parameters are fixed. The relative enhancement in the SHG is defined in the presence of the interference of the alternative absorption/emission conversion paths, due to the coupling with the attached structure by the ratio of N_{sh} to $N_{sh}^{(0)}$. N_{sh} is the total number of 2ω plasmons in the system, given in Eq. (4.16). $N_{sh}^{(0)}$ is the number of 2ω plasmons generated when the driven structure is alone. In other words, the number of 2ω plasmons generated in the presence of coupling ($f_1 \neq 0, f_2 \neq 0$), N_{sh} , to the number of 2ω plasmons in the absence of coupling ($f_1 = 0, f_2 = 0$), $N_{sh}^{(0)}$ is compared.

$$\text{Enhancement factor} \equiv \frac{N_{sh}}{N_{sh}^{(0)}} \quad (4.17)$$

The enhancement factor is calculated for varying values of ω_b for couple of parameter sets. These parameters are the coupling strengths, f_1 , and f_2 , and the damping frequency of the attached oscillator, γ_b . The unchanged parameters are the resonance frequencies of the driven oscillator, ω_1, ω_2 , the damping frequencies of the driven oscillator, γ_1, γ_2 , and the pump amplitude ε_p . So, it is investigated that how the coupling and the damping of an attached nanostructure affect the SHG of a given SH converter (driven oscillator). The results are presented in categories where the effect of changing one of the two couplings (f_1, f_2) and keeping the other fixed is displayed.

The results are presented in Figs 4.2 and 4.3. The vertical axes are the enhancement factors, and the horizontal axes are the resonance frequencies of the attached oscillator. The enhancement factor is defined by Eq. (4.17). The highest enhancement is obtained at frequencies $\omega_b = 2.01\omega$ or slightly greater than this value, in all calculations. It is observed that the enhancement factor is less than unity, which is referred as the suppression, at the frequency of the incident field, $\omega_b = 1\omega$. The reason why the SHG is suppressed at this frequency is that the linear Fano resonance does not allow excitation at the driving frequency. That is, the driving field is cancelled due to the destructive interference of multiple paths. This occurs when the driven oscillator is excited by an incident field at the frequency of the attached oscillator [14].

The enhancement factor is calculated for three different values of f_1 and f_2 , namely $f_{1,2} = 0.02$, $f_{1,2} = 0.05$, and $f_{1,2} = 0.08$. The results are gathered for different values of f_2 for $f_1 = 0.02$ in Fig. 4.2a, for $f_1 = 0.05$ in Fig. 4.2b, and for $f_1 = 0.08$ in Fig. 4.2c. It is observed that SHG is enhanced more and more with increasing f_2 , whereas changing f_1 does not affect the enhancement factor much. The enhancement factors found for different values of f_2 are more or less the same in all three graphs in Fig. 4.2. The spectral position of the enhancement is slightly shifted to the right as f_2 increases.

In order to display the effect of change in f_1 , this time, the results are gathered for different values of f_1 for $f_2 = 0.02$ in Fig. 4.3a, for $f_2 = 0.05$ in Fig. 4.3b, and for $f_2 = 0.08$ in Fig. 4.3c. These show that SHG is suppressed more and more with increasing f_1 , whereas changing f_2 does not affect the suppression factor much, since this suppression is due to linear Fano effect. The spectral position of the suppression does not change as f_1 increases.

It is concluded that the enhancement is dependent on the coupling f_2 , whereas the suppression is dependent on the coupling f_1 . This is expected because f_1 determines the strength of the coupling between the linear polarization field and the polarization on the attached nanostructure. Stronger coupling to the linear polarization field by larger values of f_1 leads to the transfer of large part of energy to the linear field rather than to the SH field. However, larger values of f_2 leads to the reverse.

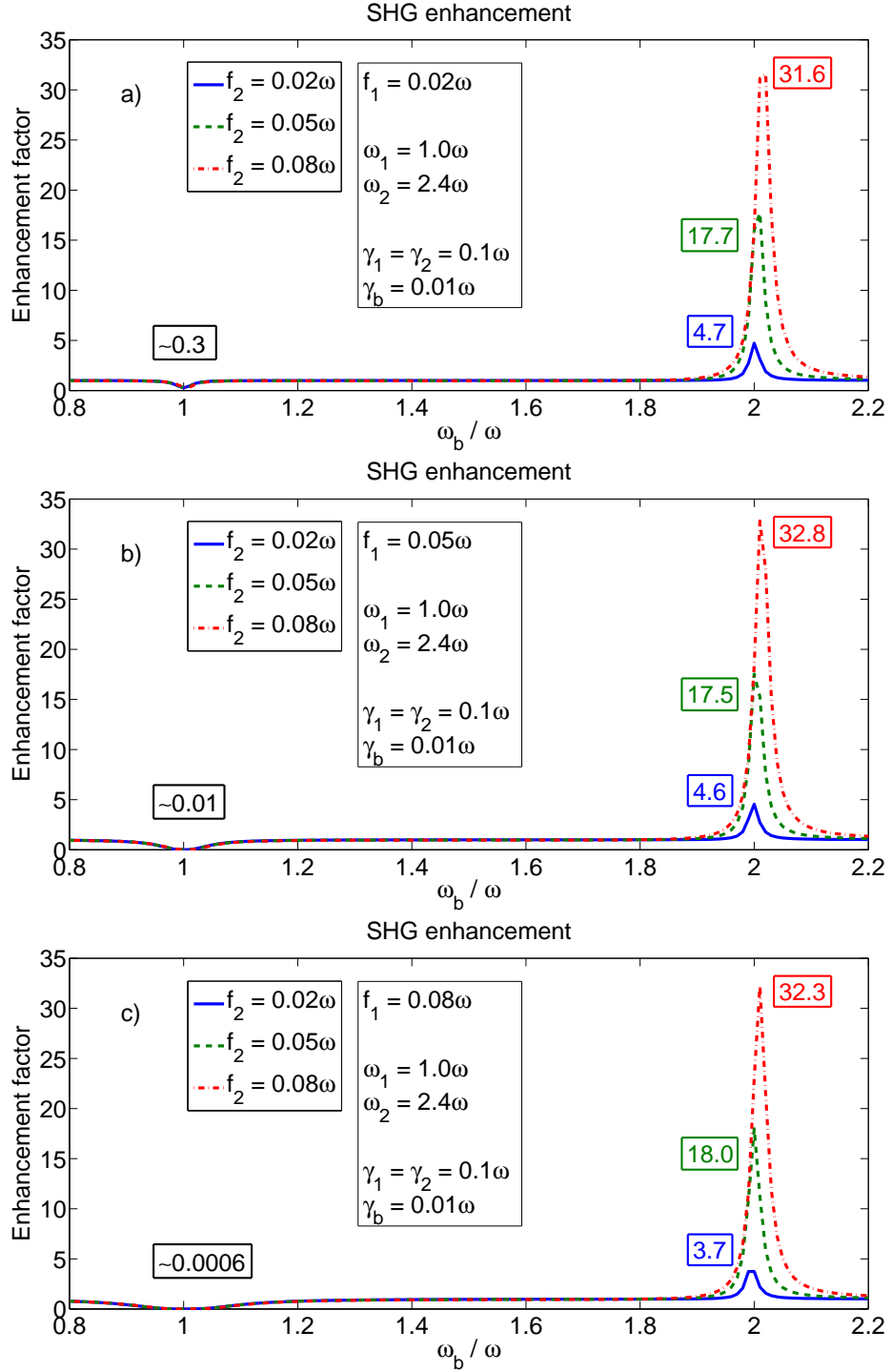


Figure 4.2: Comparison of the cases with different f_1 s (coupling between $\omega_b - \omega_1$). For all f_1 values, SHG enhancement increases with increasing f_2 . Since almost the same amount of enhancement is observed for each f_2 in all three graphs, it is reported that f_1 does not affect SHG enhancement. On the other hand it is observed that SHG response is suppressed, as f_1 increases. The spectral position of the enhancement is slightly shifted to the right as f_2 increases.

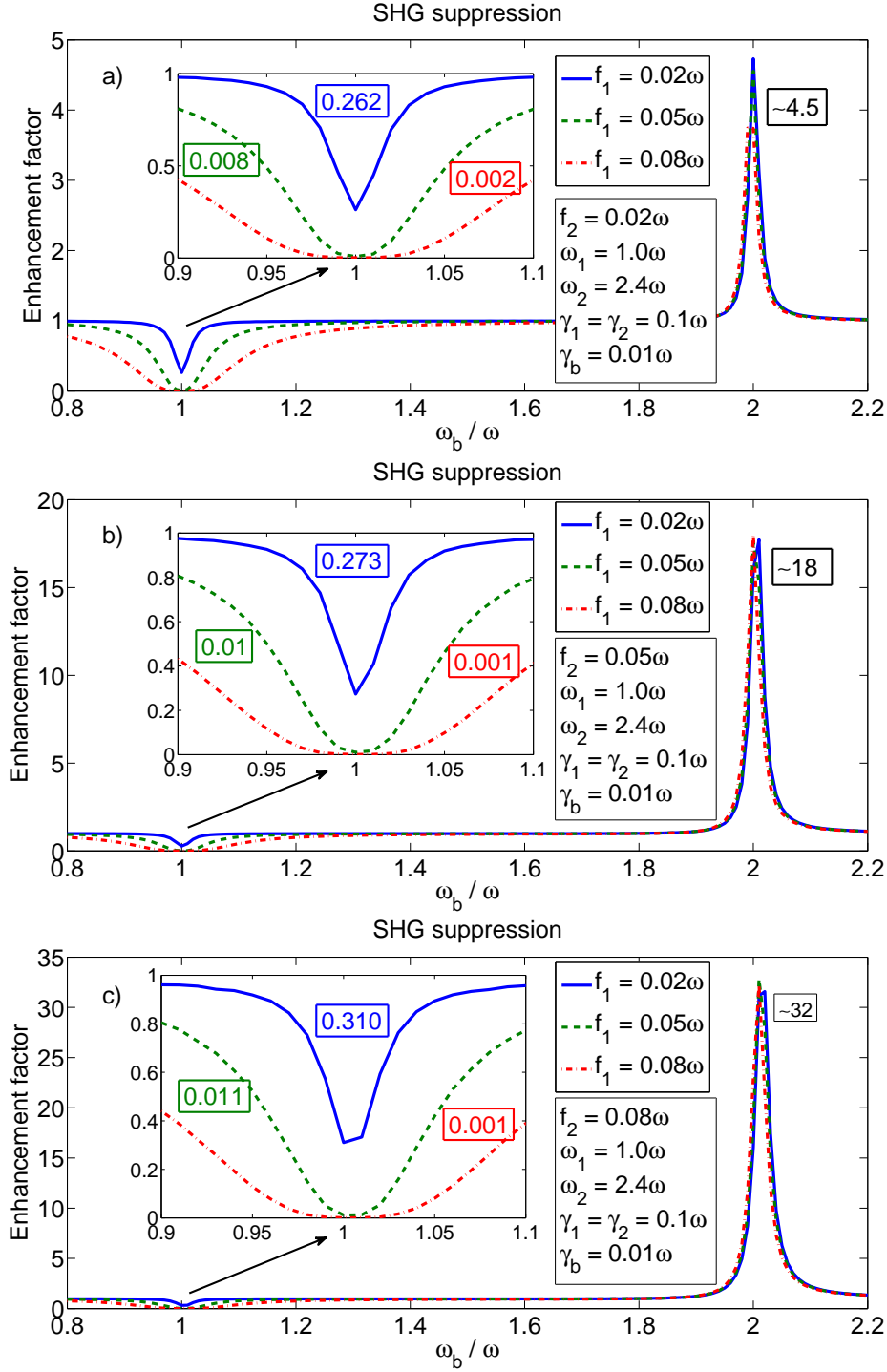


Figure 4.3: Comparison of the cases with different f_2 s (coupling between $\omega_b - \omega_2$). For all f_2 values, SHG suppression increases with increasing f_1 . Since almost the same amount of suppression is observed for each f_2 in all three graphs, it is reported that f_2 does not affect SHG suppression. On the other hand it is observed that SHG response is enhanced, as f_2 increases. The spectral position of the suppression does not change as f_1 increases.

Considering the results of subsection 3.1.1, it is suspected that increasing the coupling might not increase the enhancement for all values of the coupling. The lifetime enhancement is found to begin to decrease at some critical value of the coupling. In order to explore whether a similar phenomenon is observed for the case of SHG response, the enhancement factor is calculated for rather large values of the coupling f_2 . Moreover, in order to investigate the effect of the ratio of the damping rates of the oscillators to the value of the critical f_2 , and to the amount of the enhancement factor, these calculations are performed for two different ratio of the damping rates. The results are presented in Fig. 4.4. The enhancement factor is calculated for four different f_2 values, keeping the other parameters fixed. It is noted that the damping frequency of the attached oscillator is set to $\gamma_b = 0.001\omega$. Although a lot more data points are required in order to deduce a trend, it is shown that the stronger couplings result in less enhancement for the last three couplings. On the other hand, the results of the enhancement factor calculations for $\gamma_b = 0.01$ are shown in the inset graph of Fig. 4.4. Once again, a similar critical f_2 , as from where the enhancement factor decreases, is observed. But it is greater for the case of $\gamma_b = 0.01$, compared to the case of $\gamma_b = 0.001\omega$. In addition, comparing the main and the inset graphs in Fig.4.4, it is observed that the highest enhancement factor that can be obtained when the ratio of the damping rates is 1/10 is almost 4 times smaller than the one obtained when the ratio of the damping rates is 1/100. So, when the ratio of the damping frequencies is higher, larger enhancements can be obtained. This is one of the results of chapter 3 in the case of lifetime enhancement, and expected in consequence of Fano resonance. Another matching result with chapter 3 is that the critical coupling strength after which the response starts to decrease is smaller for the case of greater ratio of the damping rates.

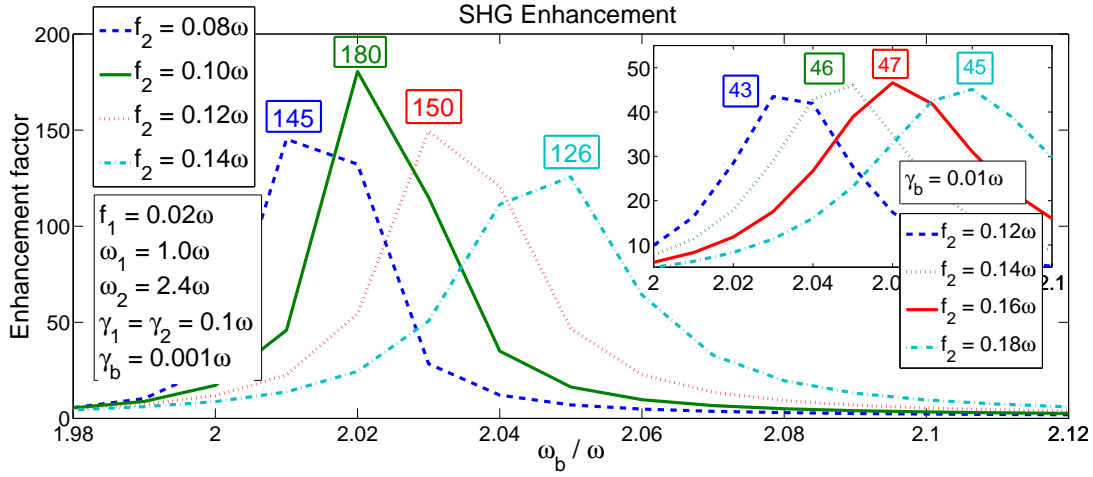


Figure 4.4: SHG enhancement for changing values of the coupling f_2 . Different curves stand for different values of f_2 . The fixed parameters are given in the figure. It is noted that $\gamma_b = 0.001\omega$ in the main graph. The highest enhancement is obtained for $f_2 = 0.10\omega$ among others. After this value, the enhancement factor starts to decrease. A similar critical f_2 , which is greater than the one in the main graph, is obtained for $\gamma_b = 0.01\omega$ in the inset graph. As one can observe, when the damping rate of the attached oscillator is higher, the highest value of the enhancement factor is higher as well.

4.2 Experimental evidence of enhancement in second harmonic response of a system of coupled plasmonic oscillators

In this section an experimental study on a similar system to the one studied within the theoretical model in 4.1, is presented. This is a system of two coupled plasmonic oscillators, a Silver nanowire (AgNW) and a Silver nanoparticle (AgNP). The sample on which the second harmonic generation (SHG) intensity is measured is shown in Fig. 4.9. A continuous wave (CW) laser source at a frequency of 1064 nm is used. While moving the focal spot (of size $\sim 1 \mu\text{m}$) of the laser stepwise along the axis of the Silver nanowire, the SHG spectrum is acquired at each step.

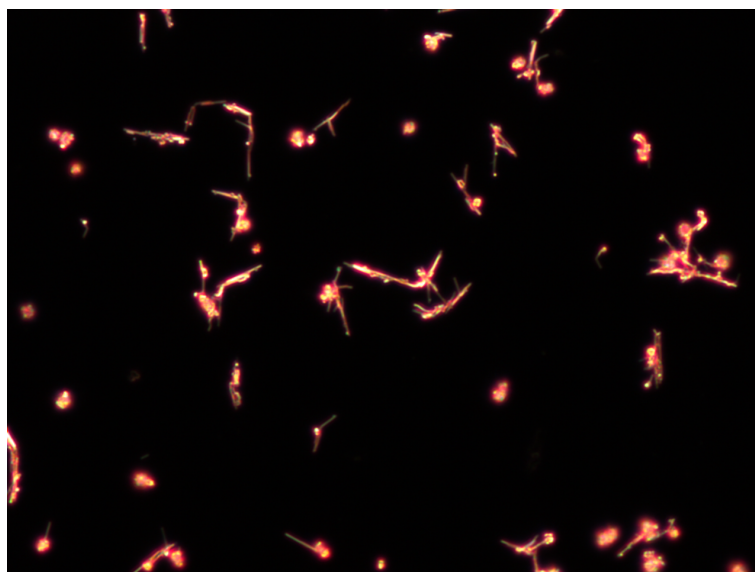


Figure 4.5: A darkfield image of the AgNW - AgNP network deposited on microscope cover-slip. Light colored long straight features in the image represent the AgNWs and the bright intense spots represent the AgNPs.

4.2.1 Colloidal solution preparation procedure

Silver nanowires are synthesized by self-seeding polyol process. In this technique, an inorganic salt is reduced by a polyol and agglomeration of particles is prevented by addition of surfactant which is commonly polyvinylpyrrolidone (PVP). Required chemicals are bought from Sigma-Aldrich. 7 mg of NaCl is added into 10 mL of 0.45 M ethylene glycol (EG) solution of PVP and heated at 170 °C. By using injection pump, solution of 0.12 M AgNO₃ in 5 mL of EG is added drop-wise at a rate of 5 mL/h. During this process, solution is stirred at 1000 rpm rate by magnetic stirrer. After the drop-wise EG addition process, solution is heated up at 170 °C for 30 minutes and is cooled to room temperature. To enable the removal of polymer from the solution, the diluted solution with acetone is centrifuged two times for 20 minutes at 6000 rpm. Afterwards, wires are dispersed in ethanol and centrifuged again under the same conditions. At the end of this procedure, nanowires with 60 nm diameter and length of 8 to 10 μm are obtained.

Solution containing bipyramids of metallic Silver is synthesized with polymer-mediated polyol process as well. 94 mM AgNO₃ is added to 3 mL EG solution. Another 3 mL

of EG solution containing 0.11 mM NaBr and 144 mM PVP is prepared and two solutions are added dropwise into heated EG solution of 5 mL in an oil bath at 160 °C which contains 30 μ L of 10 mM NaBr. After 5 hours, bipyramid solution with an average size of 150 nm is obtained [73,74]. The synthesis procedure leaves the AgNWs and AgNPs with a polymer coating of about 3-4 nm thickness.

The resulting AgNPs are co-deposited on the same substrates of AgNWs to obtain a network of NW-NP complexes, which are ultimately asymmetric structures and cover a macroscopically large area. Such coated surfaces are first imaged by dark-field microscopy to ensure the existence of the complexes (Fig. 4.5). The AgNPs are observed to display different colors such as green and blue under white light illumination as a result of their size dependent plasmon resonance in the visible range. The AgNWs are observed to show a reddish glimmer as a result of shift of their plasmon resonance towards near-infrared (NIR) due to high aspect ratio of their geometry. A combination of such two Ag nanostructures is what we expect to boost the SHG due to conversion of NIR plasmons to visible plasmons upon interaction of NWs with NPs.

4.2.2 Optical measurements

In Fig. 4.7, it is shown that the AgNWs do possess a manifold of plasmon resonances comparable to the sketched model in Fig. 4.1. The data shows differential absorption (Fig. 4.7b) which is calculated from the original absorption spectrum measurement (Fig. 4.7a) performed on a liquid dispersion of AgNWs at 0.125 mg/ml concentration. The dominant plasmon resonance [75,76] centered at 390 nm (769 THz) is subtracted from the measured data by performing a peak fit. The residual differential absorption curve (in black) is displayed in THz units to allow for direct comparison to Fig 4.1. In Fig. 4.7, three Gaussian peaks out of which two of them are much like the ω_1, ω_2 (orange solid) plasmon bands in the model are shown.

An inverted microscope (Zeiss model Axiovert 200) with a 63X (1.4 NA) objective lens is used for the experiments. In Fig. 4.6, a scheme of experimental setup is displayed. A CW Nd:YAG laser (Cobolt model Rumba) with wavelength of $\lambda = 1064$ nm and 500 mW output power is used as excitation source. The NIR signal was deliv-

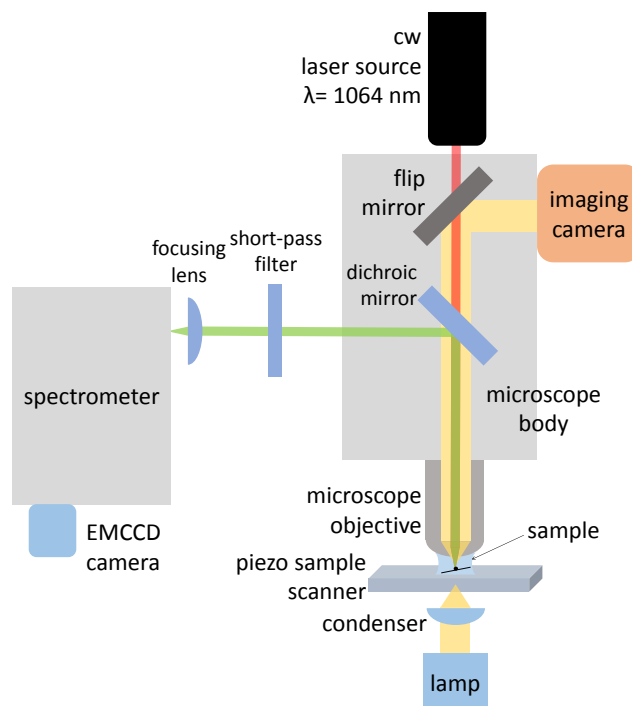


Figure 4.6: The experimental setup is composed of a CW Nd:YAG laser with $\lambda = 1064$ nm, a long-pass dichroic mirror, a flip mirror, a microscope with objective, a piezo sample scanner, a short-pass filter (cut-off at 800 nm), a focusing lens, a spectrometer with EMCCD camera, an illumination lamp, a condenser, and an imaging camera.

ered from the back port of microscope, resulting in an intensity of 40 MW/cm^2 on the sample. Resulting SHG from the AgNW-AgNP cluster was registered by a spectrometer (Andor models Shamrock 750 spectrograph + Newton 971 EMCCD (Electron Multiplying Charge Coupled Device) in corporation with a long-pass dichroic mirror cutting off the backscattered 1064 nm signal and reflecting a band of 520-750 nm.

First, a transmission image by the visual inspection camera that works in the visible is recorded, shown in Fig. 4.8. The dark figures in the image indicate the location of AgNWs, AgNPs and their clusters with a very poor resolution. Nevertheless this image is sufficient to locate a candidate region that bears a single AgNW-AgNP complex for further detailed study. The red circle on the transmission image on the left points a region of possible interest with one NW and NP complex. The red rectangle indicates the region which is scanned at a high resolution by the piezo-stage. The reflection image produced by the scanning of the same region is given on the right

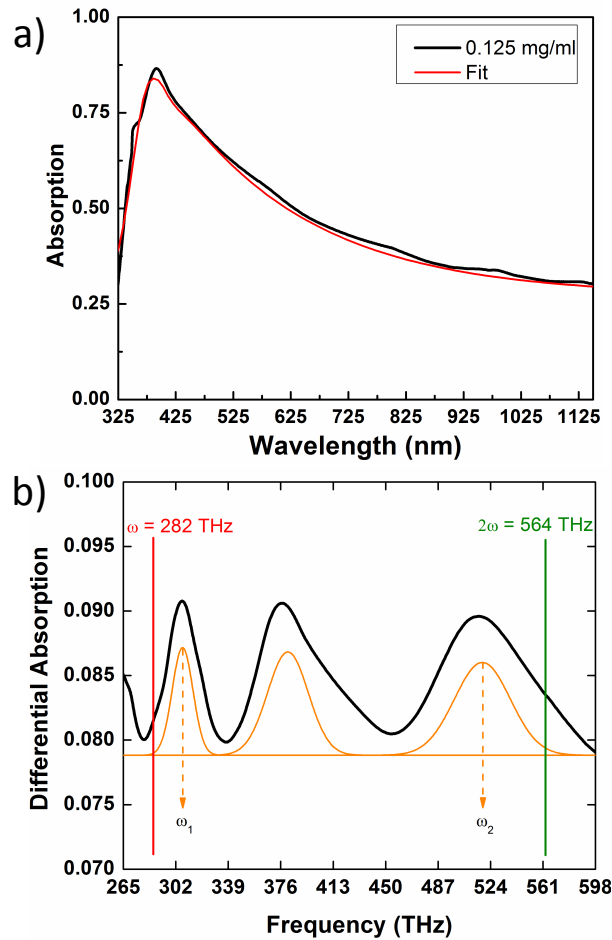


Figure 4.7: a) The absorption spectrum of liquid dispersion of AgNW (black) and a peak fit to the strongest plasmon mode at 390 nm (red). b) The differential absorption curve after the contribution of the strong plasmon peak is subtracted (black), two Gaussian peaks representing the ω_1 , ω_2 (orange solid) plasmon bands.

using a 1064 nm CW NIR laser. The reflection image produced at the illumination wavelength shows intense reflection from crowded clusters as well as a single straight feature which is the isolated part of a single AgNW and an AgNP attached towards the end of the AgNW. The faint straight shadow on the left image and a dark spot at its end appear as a straight bright feature on the left with a brighter spot at its end that indicates the attached AgNP.

Such AgNW-AgNP complexes are often encountered upon inspection of these samples with scanning electron microscope. Fig. 4.9 shows a zoomed version of the encircled straight part of the micro-scan image along with a representative sketch of

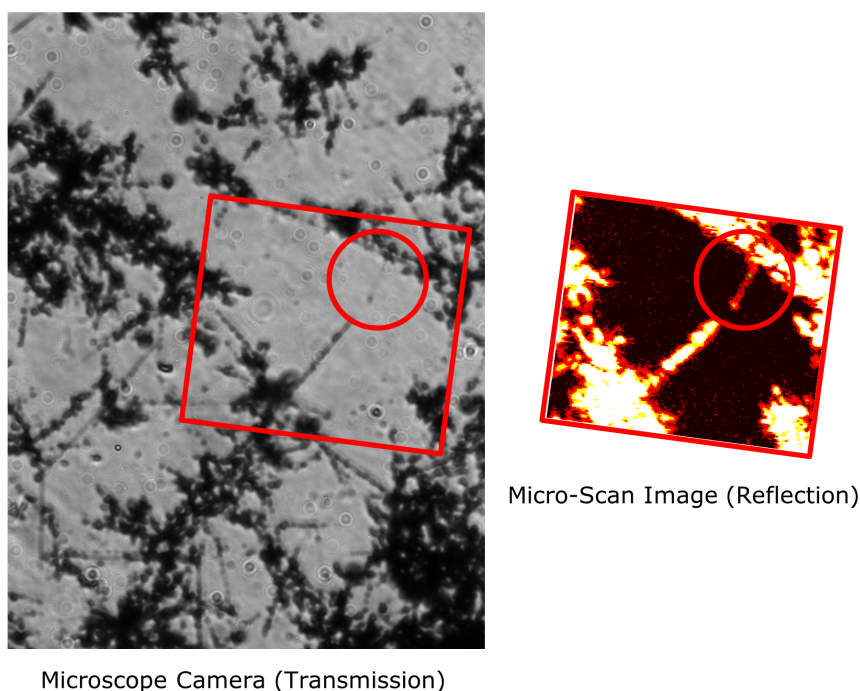


Figure 4.8: A transmission image by the microscope camera on the left and a micro-scan reflection image of the area as indicated by the red rectangle, on the right. The red circles show a region with a single AgNW with a single AgNP attached close to its end.

the AgNW-AgNP complex drawn to scale. A scanning electron microscope (SEM) image is presented on the right, that displays a highly magnified image of the end of AgNW with the attached AgNP along its body. The AgNW is typically of 50-60 nm in diameter and can be as long as 5-10 μm . The AgNPs are typically of 50-150 nm size.

4.2.3 Experimental results

By the help of the micro-scan image, the focal spot at any pixel of choice can be directed and a SHG spectra is acquired using a spectrometer EMCCD combination. While moving the diffraction limited illumination spot stepwise along the axis of the AgNW, a SHG spectrum is acquired at each step and the acquired spectra are plotted (Fig. 4.10a inset). These spectra are acquired for 60 s and integrated over SHG band. The integral SHG signal is plotted against the distance along the AgNW axis (Fig. 4.10a). The excitation polarization is linear and is in the plane of the sample surface.

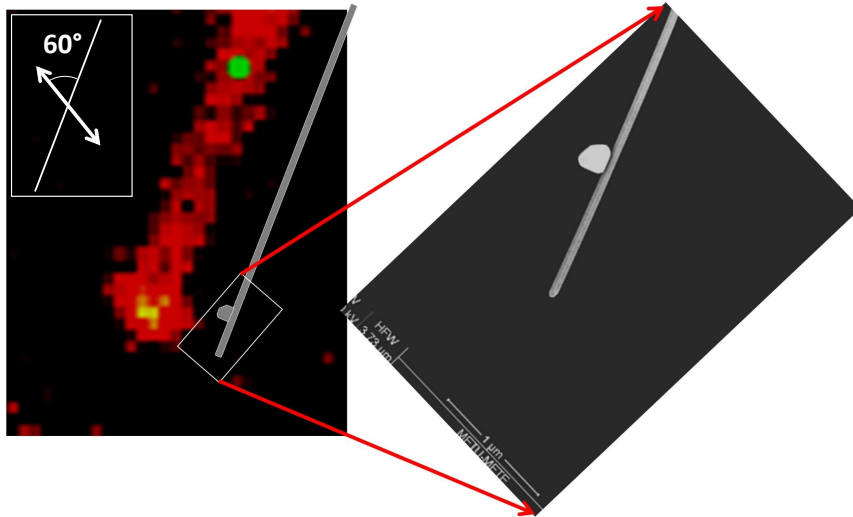


Figure 4.9: A zoom in into the encircled region in the microscan image along with a sketch of AgNW-AgNP complex. The SEM image on the right shows the end of the AgNW with high magnification.

The white arrow in the left inset in Fig. 4.9 shows the polarization direction which is 60° to this particular AgNW studied.

There are three major results obtained.

- (i) When the illumination spot is not located on the AgNW, no SHG signal is registered. So the SHG originates genuinely from the plasmonic structure.
- (ii) SHG is observed even with CW illumination (50 mW on the sample) from AgNW plasmonic structures.
- (iii) The SHG signal is enhanced by a factor of about 30 when the illumination spot is on the AgNP-AgNW complex with respect to the body of the AgNW alone.

A better visual representation of the SHG intensity distribution as a function of position along the AgNW axis is presented in Fig. 4.10b. A color bar is produced from the integral SHG signal and displayed in parallel with the actual SEM image and its representative straight extension. The SHG signal clearly appears starting from the end of the AgNW and reaches its maximum around where the AgNP is attached to the AgNW. An overlap of the color bar with a representation of such an AgNW-AgNP plasmonic hybrid complex on the right clearly depicts the observed effect: An enhanced SH conversion spot is constructed by the hybridization of the AgNW and

AgNP plasmons.

4.3 Summary and Discussion

In this chapter, enhancement of the second harmonic generation (SHG) in a system where a plasmonic second harmonic (SH) converter is coupled to an auxiliary nanoparticle, is investigated theoretically and experimentally. SHG is achieved by a nonlinear converter metal nanostructure supporting two modes with resonance frequencies close to the linear and second harmonic frequencies. The incident field excites the linear polarization mode of the SH converter. Second harmonic polarization is observed due to strongly localized polarization of the incident field. When the auxiliary particle of narrower response, is attached to the converter, it couples both to linear and second harmonic oscillation modes of the converter. This introduces conversion paths with various phases. Depending on the parameters such as the damping frequency of the attached structure, and the coupling strengths of the plasmon mode on the auxiliary particle to the modes of the converter, it is possible to obtain constructive interference at particular resonant frequencies of the auxiliary particle. This allows tuning the second harmonic response of a coupled plasmonic system.

In section 4.1, a theoretical model examining the second harmonic generation via a coupled plasmonic system is developed. In order to observe Fano resonances, one of the oscillators should support a mode with a longer lifetime than that of the other. This is the attached particle in the theoretical model. Plasmonic modes are treated as quantum harmonic oscillators. Hamiltonian of the system is defined and the Heisenberg equations for the oscillation amplitudes are derived. The coupled differential equations are numerically time evolved until a steady state has been reached, to obtain the total number of second harmonic (2ω) plasmons. The enhancement factor is defined by the total number of 2ω plasmons in the case of coupling to the auxiliary particle, normalized to the one calculated in the absence of the coupling. What it is referred as the suppression is the case when the enhancement factor is less than unity. SHG enhancement (and suppression) is obtained for varying values of the resonance frequencies of the attached oscillator (ω_b), for couple of parameter sets. These parameter sets include different values of the couplings f_1 , f_2 , and the damping of the

attached structure, γ_b . The results are displayed in Figs. 4.2, 4.3, and 4.4.

According to these results, it is concluded that the amount of SHG enhancement depends on f_2 , the strength of the coupling of the attached structure to the ω_2 mode of the converter, where SHG emerges. On the other hand, SHG enhancement is independent of f_1 , the strength of the coupling of the attached structure to the linear polarization field (ω_1 mode). On the contrary, the amount of the suppression of the SH response is determined by f_1 , whereas f_2 does not change it. It is noted that, no suppression is observed at $\omega_b = 2\omega$ unlike the case where the auxiliary particle is a quantum emitter [20]. This is due to the presence of the coupling between ω_b and ω_1 modes.

In addition, the amount of the enhancement increases the ratio of the damping rates of the structure is increased. This is an expected result, as Fano resonances become much stronger when the damping of one of the oscillators are much smaller. In an alternative picture, this is also related with the enhancement of the lifetime of the ω_2 mode by the coupling to the auxiliary particle. It is enhanced more when γ_b is smaller. It is found that the highest SHG enhancement is almost 4 times larger in the case where $\gamma_b = 0.001\omega$, compared to the case where $\gamma_b = 0.01\omega$, (Fig. 4.4), where ω is the frequency of the incident field, and all frequencies are scaled to this value.

The spectral positions of the enhancements are found at frequencies slightly larger than $\omega_b = 2\omega$. As the coupling with ω_2 mode, f_2 is increased, it is observed that the spectral position of the enhancement slightly shifts to the higher frequencies. On the other hand, it is observed that the SHG is suppressed at $\omega_b \approx 1\omega$ for all parameter sets used. This is because the linear Fano resonance does not allow excitation at the driving frequency.

The comparison of the graphs given in Fig. 4.4 shows that, similar to the lifetime of the linear polarization examined in chapter 3, SHG enhancement starts to decrease after a critical value of the coupling. And similarly to the case of lifetime enhancement, this critical coupling value is smaller when the ratio of the damping frequencies are larger.

In section 4.2, an experimental study on a similar plasmonic system of Silver nanos-

structures is presented. In the experiment, Silver nanoparticle and nanowire samples are illuminated with continuous wave near-infrared (NIR) laser source of 1064 nm wavelength at different focal points with a focal spot of 1 μm diameter. First, AgNW and AgNP samples of typical sizes 5 μm and 100 nm, respectively, are illuminated separately and second harmonic (SH) response is recorded. Second, the two MNSs are combined and a representative coupled MNS system is identified. The focus of NIR laser is moved stepwise along the axis and the SH response at 532 nm wavelength is recorded at each step (Fig. 4.10). It is observed that when the laser focus is in the region containing the coupled AgNP, the SH signal is enhanced up to about 30 times as compared to the AgNP-free regions on the AgNW axis.

The amount of enhancement observed in the experiment matches with the results of the theoretical model shown by the red dashed curves in Fig. 4.2. The oscillation parameters used in these calculations, namely the damping frequencies and coupling strengths can be compared and associated to the ones in the experiment. This can provide foresight for the future experiments of different parameters.

The attached MNS has a distorted bipyramidal shape and can support dark modes [36] with relatively longer lifetimes than that of bright modes. Therefore, in the experiment AgNW plays the role of SH converter and bipyramid AgNP is the attached higher quality plasmonic oscillator. This is also confirmed by the control experiments performed on AgNW and AgNP samples separately, where the former is found to generate ~ 6 times higher SH conversion, compared to the latter. It can be noted that the AgNP size effect is incorporated to the model partially through the f_1 and f_2 parameters in Eq. (4.3). AgNPs with different sizes are expected to have different ω_b positions which results in different levels of overlaps between ω_1 and ω_2 and hence different magnitudes of f_1 and f_2 , respectively. The magnitudes of these parameters play an important role in the SHG enhancement.

Alzar et. al. 2002, show that absorption cancellations due to Fano resonances can be achieved in entirely classical systems [34]. This is observed in the experiment covered in section 4.2 and in some recent experiments [19, 24, 28–30]. The enhancement/suppression effects on the spectrum of the nonlinear conversion are revealed using very simple arguments.

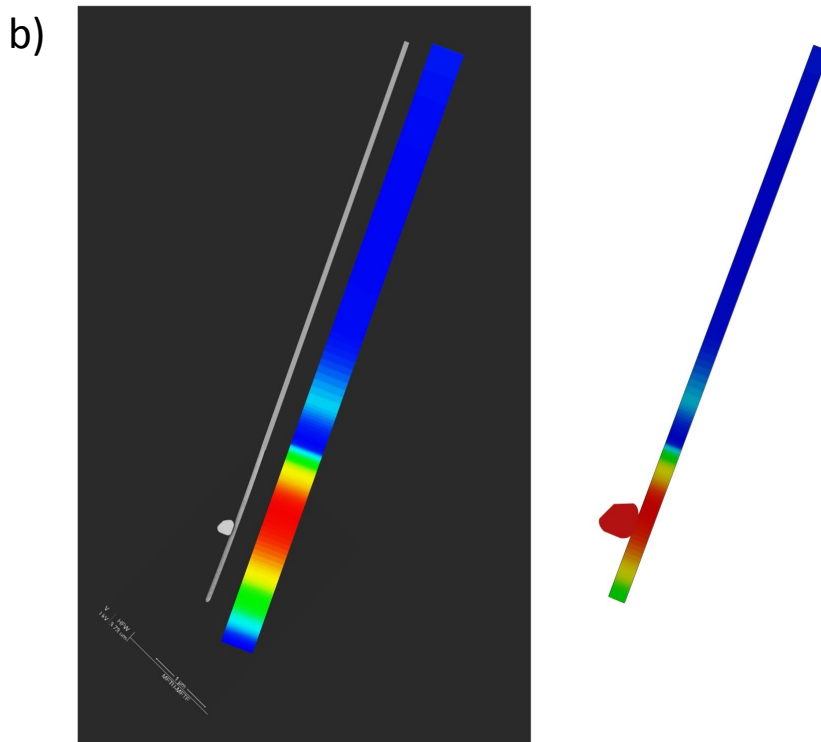
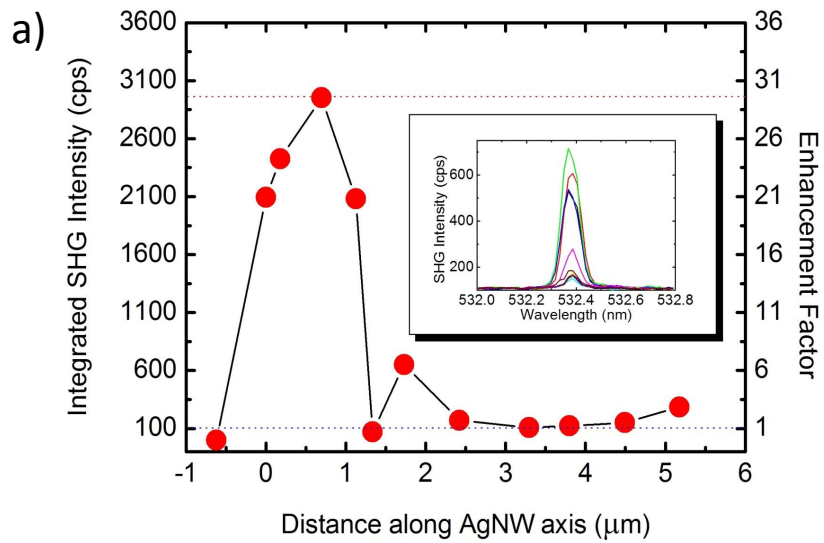


Figure 4.10: a) The SHG spectra obtained at different positions along the body of the AgNW (inset). The integrated SHG intensity (left vertical axis) and the enhancement factor (right vertical axis) as a function of position on the AgNW. The breadth of the SHG signal peak along the AgNW axis is due to the $1 \mu\text{m}$ focal spot size. b) The SHG integral signal intensity as a color bar and the AgNW along with it, clearly show that the enhancement originates from coupling of the AgNW with the AgNP. The color bar superposed onto the representative sketch of the system -on the right.

CHAPTER 5

CONCLUSIONS

Metal nanostructures (MNSs) can confine the incident field into nanoscale dimensions, improving trapping properties or effective optical thicknesses of dielectric structures [77]. This thesis focuses on the effects of Fano resonances in coupled plasmonic systems of MNSs. The effects of the coupling on linear polarization lifetime and second harmonic (SH) polarization response are investigated. The aim is to obtain a foresight of effective use of MNSs in photonic-electronic applications. The lifetime of a linear polarization mode of a coupled system, and the intensity of SH response generated by a coupled system are examined in detail in chapters 3 and 4, respectively.

In both chapters, a system of two coupled plasmonic nanostructures is investigated. The condition for observing Fano resonance in a coupled system is that one of the oscillators should have a longer lifetime than the other. So, such coupled systems are considered. The aim is to enhance the response of the system by utilizing the coupling effects. What it is meant by the response is the lifetime of the linear polarization for chapter 3, and the intensity of second harmonic polarization field for chapter 4. The incident field cannot excite the longer lifetime oscillator, as it is a dark mode or/and nonresonant with the incident field in chapter 3. So, despite supporting a long-lived polarization, it cannot be excited without being attached to a driven oscillator. It is excited by near-field interaction. In chapter 4, the long lifetime oscillator is not a second harmonic converter, as it supports only a single mode. Hence, it is useless for generation of second harmonic plasmons when it is alone. So common to both problems, the short lifetime oscillator is utilized to excite the system, and the long lifetime oscillator, to enhance the response.

In chapter 3, the lifetime of linear polarization fields of a coupled plasmonic system is examined using two different approaches. In the first approach, the plasmonic structures are treated as quantum harmonic oscillators excited by classical electromagnetic fields. An eigenvalue equation consisting of coupled differential equations describing the dynamics of the system is obtained. The lifetime is defined as the mean value of the oscillation time, weighted over plasmon intensity, by Eq. (3.29). Solving the eigenvalue equation, it is demonstrated that the lifetime of a plasmonic system can be enhanced by factors depending on the oscillation parameters. Lifetime of the coupled system is obtained for varying coupling strengths, f , for couple of parameter sets. The value of one of the oscillation parameters is systematically changed while keeping the others fixed, and the relationship between the lifetime and the associated parameter is examined. The parameters are the resonance frequencies, $\omega_{1,2}$, the damping rates of the oscillators, $\gamma_{1,2}$, and the coupling strength, f . The oscillation durations of the system in the short term and long term are examined separately. The results are presented in Fig.s 3.3- 3.9. The major conclusions are the following.

- (i) For fixed damping rates, no matter what the resonance frequencies are, the amount of the highest lifetime that the system achieves is the same. On the other hand, as the detuning between the resonance frequencies of the oscillators increase, the system requires a stronger coupling, f , to obtain the same maximum lifetime (Fig.s 3.3-3.6)
- (ii) The resonance frequencies are symmetric. (For instance in Fig. 3.3 and 3.4, exactly the same results are obtained, when the resonance frequencies, $\omega_{1,2} = \omega_{2,1}$ are switched.)
- (iii) The highest lifetime obtained increases, as the ratio of the damping rates of the oscillators increases. (Compare Fig. 3.3 with Fig. 3.5, and Fig. 3.4 with Fig. 3.6.)
- (iv) In the long term behaviour, the lifetime extends with increasing coupling, up to a critical value of the coupling at first, then declines, and finally becomes constant. This particular value is smaller when the ratio of the damping rates is larger. (Fig.s 3.3-3.6)
- (v) The lifetime is not extended much in the short term integration of Eq. (3.29), because the final saturated enhancement can not be obtained at the earlier times of the coupling. The decay is governed by a smaller amplitude and a much smaller rate in the long term. The plasmons continue to count up for longer times (Fig.s 3.7-3.8).

In the second approach, the coupled plasmonic system is treated as a classical electromagnetic problem. The Maxwell's equations are numerically solved by finite difference time domain (FDTD) method using MEEP. The lifetime of the plasmonic oscillator is defined by the decay time of the near-field energy in a box enclosing the structure (see Fig. 3.10), when the source leaves the region. Two cases are examined: (i) the case when the plasmonic oscillator is alone, and (ii) the case when an additional particle is attached to it. Doing so, in addition to the analytical demonstration presented as the first approach, additionally, a 3D Maxwell solution is provided as a demonstration of the lifetime enhancement via coupled plasmonic oscillators. It is observed that when first metal nanostructure (MNS1) is alone, the near-field energy decays immediately after the source leaves the structure, corresponding to lifetime of 0.168 fs as shown in Fig. 3.12a. When the second metal nanostructure (MNS2) of longer lifetime, is attached to the system, the near-field energy decays as a superposition of two different decay rates, corresponding to lifetimes of 0.157 fs and 11.42 fs, as shown in Fig. 3.12b. It is noted that the lifetime obtained in this section is defined as the *near-field* decay time. However, it is common to define the lifetime as the *far-field* decay time. Therefore the lifetime values obtained in this section are smaller than the ones encountered in the literature. The energy of the coupled system decays very rapidly at first, i. e., the decay is governed by a higher rate. However, Fig. 3.12b shows that it remains almost constant after this rapid drop to ~ 10 percent of its initial value. A different decaying rate governs the evolution. Comparing this with the other system where MNS1 is alone, the polarization lasts for a ~ 70 times longer duration. The long term behaviour of the near-field energy, obtained in section 3.2, matches with the long term behaviour of the oscillation amplitudes calculated in section 3.1 (See Fig. 3.9).

By numerically solving the Maxwell's equations, the scattering cross sections are obtained for MNS1 and MNS2 separately, and for the coupled system of these two structures (see Fig. 3.13). It is observed that the peak for the linear response of MNS2 is shifted to the left (to shorter wavelengths). This shows the presence of a weak hybridization. Because, it was a superposition rather than hybridization, the response peak of MNS2 would shift to the right, where the the response of MNS1 is higher. Furthermore, it is observed that the response of MNS2 is broadened, while that of

MNS1 is slightly sharpened. Under the light of these observations, it is concluded that weakly hybridized modes are obtained on these plasmonic particles of distinct damping rates, leading to an enhanced lifetime for MNS1, and a suppressed lifetime for MNS2.

In chapter 4, a theoretical model examining second harmonic generation from a coupled system of two MNSs is developed and an experimental study on a Silver nanowire (AgNW) - Silver nanoparticle (AgNP) system is reported. The plasmonic system examined consists of two MNSs, one of which has a longer lifetime than the other, but cannot generate second harmonic polarization. The short lifetime oscillator is a second harmonic converter and it is excited by an incident field resonantly. The attached long lifetime structure is utilized to enhance the number of second harmonic plasmons by introducing phase-varying conversion paths as a result of coupling with the converter structure.

Alzar et. al. 2002, [34] demonstrate the classical analog of electromagnetically induced transparency where absorption/emission paths of a coupled quantum system is cancelled. This results in a dip in the linear response spectrum for a coupled harmonic oscillator system driven by a harmonic field. Türkpençe et. al. 2014 [20], demonstrate that second harmonic generation from a plasmonic converter can be enhanced by coupling it with a quantum emitter. They explicitly display the cancelling of the nonresonant terms in the nonlinear response function. In this study, in chapter 4, a similar route is followed to demonstrate this phenomenon in the nonlinear response of a coupled *all-plasmonic* system [78]. The second harmonic generation is examined by developing a theoretical model based on the solutions of differential equations, treating the plasmonic oscillators as harmonic oscillators driven by an incident electromagnetic field. SHG enhancement factor is defined as the total number of second harmonic plasmons summed over the modes, normalized to the one when there is no coupling. Magnitudes of the following parameters play an important role on the amount of the enhancement obtained. f_1 and f_2 stand for the overlaps of the mode supported by the attached oscillator, ω_b , with the linear and second harmonic polarization modes supported by the converter, respectively. The enhancement factors are obtained for varying resonance frequencies of the long-lived attached oscillator. It is shown that the second harmonic generation can be enhanced by factors depending on

the coupling parameters such as the damping frequency, γ_b , of the attached oscillator, and the coupling coefficients of the attached oscillator's mode, f_1 and f_2 , between the driven (linear) and the second harmonic polarization modes, respectively. Structures with different geometries are expected to have different resonance frequencies, ω_b , and that should result in different levels of overlaps of ω_b with ω_1 and ω_2 and hence different magnitudes of f_1 and f_2 , respectively. Therefore the enhancement factor is calculated for different f_1 and f_2 values to obtain an optimal coupling strength for SHG enhancement. Handling the problem within a very simple approach, four major conclusions are obtained.

(i) SHG enhancement increases with increasing values of the coupling f_2 , whereas is independent from the coupling f_1 (Fig. 4.2).

(ii) SHG suppression increases with increasing values of the coupling f_1 , whereas is independent from the coupling f_2 (Fig. 4.3).

(iii) The amount of SHG enhancement is greater when the ratio of the damping rates of the oscillators are higher (Fig. 4.4).

(iv) SHG enhancement increases with increasing f_2 up to a critical value, and then decreases. This value is a smaller value for the case when higher ratio of the damping rates is used (Fig. 4.4).

The outcomes expressed in items (iii) and (iv), above, match with the ones in the items with the same numbers for chapter 3. It is observed that the enhancements in the lifetime of the linear polarization and in the intensity of the nonlinear polarization are higher when the ratio of the damping rates of the oscillators are higher too.

A somewhat surprising conclusion is the one expressed in item (iv). As the strength of the Fano-coupling is raised, one may expect a stronger response. However the calculations demonstrate that, after some certain value of the coupling strength, this positive relation is destroyed for both responses calculated in chapters 3 and 4. That is, after some critical coupling, the response starts to decrease with increasing coupling. In both calculations, this critical value is smaller in the case of high ratio of the damping rates.

In the last part of chapter 4, an experimental study on the second harmonic response of a coupled plasmonic system of Silver nanostructures is presented. In the experiment,

AgNP-AgNW sample is illuminated with a continuous wave laser of $\lambda=1064$ nm at various focal points along the wire axis, with a focal spot size of $1 \mu\text{m}$. AgNW and AgNP samples of typical sizes $5 \mu\text{m}$ and 100 nm, respectively, are illuminated separately as control measurements and second harmonic signal is recorded. Then the two MNSs are combined and a representative coupled MNS is identified (Fig. 4.8). The source is focused stepwise along the wire axis and the second harmonic response at 532 nm wavelength is recorded at each step (Fig. 4.10). The attached nanostructure, i.e., AgNP, has a distorted bipyramidal shape and can support dark modes [36] with relatively longer lifetimes than that of bright modes. Therefore, analogically, AgNW plays the role of SH converter MNS with short lifetime, and bipyramidal shape AgNP is the attached higher quality plasmonic oscillator. This is also confirmed by the control measurements performed on AgNW and AgNP samples separately, where the former is found to generate ~ 6 times higher second harmonic conversion. It is observed that the second harmonic signal at $\lambda=532$ nm is ~ 30 times higher at the position of the laser spot on the AgNP-AgNW complex, compared to the points along the AgNW axis. This much enhancement is reasonably obtained in the theoretical model as the enhancement factor of ~ 32 , shown in Fig. 4.3, for a parameter set of $\gamma_{1,2} = 0.1\omega$, $\gamma_b = 0.01\omega$, $f_2 = 0.08\omega$. The outcomes of the theoretical model can be used to predict the properties of future experiments, by matching the conditions of the presented experiment with the coupling parameters used in the theoretical model.

As a final word, it is presented a thesis investigating the effects of Fano resonances on the lifetime of the linear polarization and the intensity of the second harmonic polarization for a coupled plasmonic oscillator system. The enhancements of the responses are theoretically demonstrated by relating them with the parameters of the oscillations. An experimental evidence for the enhancement of second harmonic generation of a plasmonic converter is presented as a result of plasmonic coupling.

REFERENCES

- [1] E. Hutter and J. Fendler, “Exploitation of localized surface plasmon resonance.,” *Advanced Materials*, vol. 16, no. 19, pp. 1685–1706, 2004.
- [2] M. I. Stockman, “Nanoplasmonics: Past, present, and glimpse into future.,” *Optics Express*, vol. 19, no. 22, pp. 22029–22106, 2011.
- [3] J. N. Anker, W. P. Hall, O. Lyandres, N. C. Shah, J. Zhao, and R. P. Van Duyne, “Biosensing with plasmonic nanosensors.,” *Nature Materials*, vol. 7, no. 6, pp. 442 – 453, 2008.
- [4] D. Dregely, R. Taubert, J. Dorfmüller, R. Vogelgesang, K. Kern, and H. Giessen, “3d optical yagi-uda nanoantenna array.,” *Nature Communications*, vol. 2, 2011.
- [5] A. Ono, J.-I. Kato, and S. Kawata, “Subwavelength optical imaging through a metallic nanorod array.,” *Physical Review Letters*, vol. 95, no. 26, p. 267407, 2005.
- [6] F. Tam, G. P. Goodrich, B. R. Johnson, and N. J. Halas, “Plasmonic enhancement of molecular fluorescence.,” *Nano Letters*, vol. 7, no. 2, pp. 496 – 501, 2007.
- [7] V. G. Kravets, F. Schedin, R. Jalil, L. Britnell, R. V. Gorbachev, D. Ansell, B. Thackray, K. S. Novoselov, A. K. Geim, A. V. Kabashin, and A. N. Grigorenko, “Singular phase nano-optics in plasmonic metamaterials for label-free single-molecule detection.,” *Nature Materials*, vol. 12, no. 4, pp. 304 – 309, 2013.
- [8] M. Kauranen and A. V. Zayats, “Nonlinear plasmonics.,” *Nature Photonics*, vol. 6, no. 11, pp. 737 – 748, 2012.
- [9] C. D. Geddes, *Reviews in Plasmonics*. New York, NY : Springer New York, 2015.
- [10] X. Wu, S. K. Gray, and M. Pelton, “Quantum-dot-induced transparency in a nanoscale plasmonic resonator,” *Opt. Express*, vol. 18, no. 23, pp. 23633–23645, 2010.
- [11] A. Melikyan and H. Minassian, “On surface plasmon damping in metallic nanoparticles.,” *Applied Physics B: Lasers and Optics*, vol. 78, no. 3/4, pp. 453 – 455, 2004.

- [12] M. A. Noginov, G. Zhu, A. M. Belgrave, S. Stout, R. Bakker, V. M. Shalaev, E. E. Narimanov, E. Herz, T. Suteewong, and U. Wiesner, “Demonstration of a spaser-based nanolaser.,” *Nature*, vol. 460, no. 7259, pp. 1110–1112, 2009.
- [13] T. Jonathan G., W. Anthony J., T. Chaker, C. Ilenia, E. Stuart W. J., R. Alan J., K. Mizanur R., G. Peter, M. Andrew R., C. Colin J., B. Till T., G. Gerard, S. Holger, and C. Jason, “Fluorescence lifetime imaging of quantum dot labeled dna microarrays.,” *International Journal of Molecular Sciences, Vol 10, Iss 4, Pp 1930-1941 (2009)*, no. 4, p. 1930, 2009.
- [14] A. E. Miroshnichenko, Y. S. Kivshar, and S. Flach, “Fano resonances in nanoscale structures.,” *Reviews of Modern Physics*, vol. 82, no. 3, pp. 2257–2298, 2010.
- [15] M. E. Tasgin, “Metal nanoparticle plasmons operating within a quantum lifetime.,” *Nanoscale*, vol. 5, no. 18, pp. 8616 – 8624, 2013.
- [16] T. Hoang, J. Huang, D. Smith, M. Mikkelsen, G. Akselrod, and C. Argyropoulos, “Ultrafast spontaneous emission source using plasmonic nanoantennas.,” *Nature Communications*, vol. 6, 2015.
- [17] S. Bidault, A. Devilez, V. Maillard, L. Lermusiaux, J.-M. Guigner, N. Bonod, and J. Wenger, “Picosecond lifetimes with high quantum yields from single-photon-emitting colloidal nanostructures at room temperature,” *ACS Nano*, vol. 10, no. 4, pp. 4806–4815, 2016.
- [18] T. K. Hakala, H. T. Rekola, A. I. Väkeväinen, J. P. Martikainen, A. J. Moilanen, and P. Törmä, “Lasing in dark and bright modes of a finite-sized plasmonic lattice.,” 2016.
- [19] B. Luk’yanchuk, N. I. Zheludev, S. A. Maier, N. J. Halas, P. Nordlander, H. Giessen, and C. T. Chong, “The fano resonance in plasmonic nanostructures and metamaterials,” *Nature materials*, vol. 9, no. 9, pp. 707–715, 2010.
- [20] D. Turkpence, M. E. Tasgin, G. B. Akguc, and A. Bek, “Engineering nonlinear response of nanomaterials using fano resonances.,” *Journal of Optics*, vol. 16, no. 10, p. 105009, 2014.
- [21] M. Tasgin, I. Salakhutdinov, M. Abak, A. Bek, D. Kendziora, L. Fruk, D. Turkpence, L. Piantanida, and M. Lazzarino, “Fluorescence excitation by enhanced plasmon upconversion under continuous wave illumination.,” *Photonics and Nanostructures - Fundamentals and Applications*, vol. 21, pp. 32–43, 2016.
- [22] B. Sharma, R. R. Frontiera, A.-I. Henry, E. Ringe, and R. P. Van Duyne, “Sers: Materials, applications, and the future.,” *Materials Today*, vol. 15, no. 1-2, p. 16, 2012.

- [23] P. Genevet, J. P. Tetienne, M. A. Blanchard, R. and Kats, F. Capasso, E. Gatzogiannis, and M. O. Scully, “Large enhancement of nonlinear optical phenomena by plasmonic nanocavity gratings.,” *Nano Letters*, vol. 10, no. 12, pp. 4880–4883, 2010.
- [24] J. Renger, R. Quidant, and L. Novotny, “Enhanced nonlinear response from metal surfaces,” *Opt. Express*, vol. 19, no. 3, pp. 1777–1785, 2011.
- [25] J. D. Cox, M. R. Singh, C. von Bilderling, and A. V. Bragas, “A nonlinear switching mechanism in quantum dot and metallic nanoparticle hybrid systems,” *Advanced Optical Materials*, vol. 1, no. 6, pp. 460–467, 2013.
- [26] J. D. Cox, M. R. Singh, M. A. Anton, and F. Carreno, “Plasmonic control of nonlinear two-photon absorption in graphene nanocomposites,” *Journal of Physics: Condensed Matter*, vol. 25, no. 38, p. 385302, 2013.
- [27] C. Racknor, M. R. Singh, Y. Zhang, D. J. S. Birch, and Y. Chen, “Energy transfer between a biological labelling dye and gold nanorods,” *Methods and Applications in Fluorescence*, vol. 2, no. 1, p. 015002, 2014.
- [28] K. Thyagarajan, J. Butet, and O. J. F. Martin, “Augmenting second harmonic generation using fano resonances in plasmonic systems.,” *Nano Letters*, vol. 13, no. 4, pp. 1847–1851, 2013.
- [29] J. Berthelot, M. Song, P. Rai, G. C. Des Francs, A. Dereux, A. Bouhelier, and G. Bachelier, “Silencing and enhancement of second-harmonic generation in optical gap antennas.,” *Optics Express*, vol. 20, no. 10, pp. 10498–10508, 2012.
- [30] S. Wunderlich and U. Peschel, “Plasmonic enhancement of second harmonic generation on metal coated nanoparticles.,” *Optics Express*, vol. 21, no. 16, pp. 18611 – 18623, 2013.
- [31] S. Gao, K. Ueno, and H. Misawa, “Plasmonic antenna effects on photochemical reactions.,” *Accounts of Chemical Research*, vol. 44, no. 4, pp. 251–260, 2011.
- [32] M. R. Singh, “Enhancement of the second-harmonic generation in a quantum dot-metallic nanoparticle hybrid system.,” *Nanotechnology*, vol. 24, no. 12, pp. 125701 – 125706, 2013.
- [33] G. F. Walsh and L. Dal Negro, “Enhanced second harmonic generation by photonic-plasmonic fano-type coupling in nanoplasmonic arrays.,” *Nano Letters*, vol. 13, no. 7, p. 3111, 2013.
- [34] C. L. G. Alzar, M. A. G. Martinez, and P. Nussenzeig, “Classical analog of electromagnetically induced transparency.,” *American Journal of Physics*, no. 1, p. 37, 2002.

- [35] P. Tassin, L. Zhang, R. Zhao, A. Jain, T. Koschny, and C. M. Soukoulis, “Electromagnetically induced transparency and absorption in metamaterials: The radiating two-oscillator model and its experimental confirmation.,” *Physical Review Letters*, vol. 109, no. 18, p. 187401, 2012.
- [36] S. Panaro, A. Nazir, C. Liberale, G. Das, H. Wang, F. De Angelis, R. Proietti Zaccaria, E. Di Fabrizio, and A. Toma, “Dark to bright mode conversion on dipolar nanoantennas: a symmetry-breaking approach,” *ACS Photonics*, vol. 1, no. 4, pp. 310–314, 2014.
- [37] A. Artar, A. A. Yanik, and H. Altug, “Multispectral plasmon induced transparency in coupled meta-atoms.,” *Nano Letters*, vol. 11, no. 4, pp. 1685–1689, 2011.
- [38] A. E. Cetin, A. Artar, M. Turkmen, A. A. Yanik, and H. Altug, “Plasmon induced transparency in cascaded p-shaped metamaterials.,” *Optics Express*, vol. 19, no. 23, pp. 22607–22618, 2011.
- [39] R. Wood, “On a remarkable case of uneven distribution of light in a diffraction grating spectrum.,” *Philosophical Magazine*, vol. 4, no. 19-24, pp. 396 – 402, 1902.
- [40] L. Rayleigh, “Note on the remarkable case of diffraction spectra described by prof. wood.,” *Philosophical Magazine*, vol. 14, no. 79-84, pp. 60 – 65, 1907.
- [41] L. Rayleigh, “On the dynamical theory of gratings.,” *Proceedings of the Royal Society of London. Series A, Containing Papers of a Mathematical and Physical Character*, no. 532, p. 399, 1907.
- [42] U. Fano, “The theory of anomalous diffraction gratings and of quasi-stationary waves on metallic surfaces (sommerfeld’s waves).,” *Journal of the Optical Society of America (1917-1983)*, vol. 31, no. 3, p. 213, 1941.
- [43] R. H. Ritchie, “Plasma losses by fast electrons in thin films,” *Phys. Rev.*, vol. 106, pp. 874–881, Jun 1957.
- [44] E. A. Stern and R. A. Ferrell, “Surface plasma oscillations of a degenerate electron gas,” *Phys. Rev.*, vol. 120, pp. 130–136, 1960.
- [45] A. Otto, “Excitation of nonradiative surface plasma waves in silver by the method of frustrated total reflection,” *Zeitschrift für Physik A Hadrons and nuclei*, vol. 216, no. 4, pp. 398–410, 1968.
- [46] E. Kretschmann and H. Raether, “Radiative decay of non radiative surface plasmons excited by light.,” *Zeitschrift für Naturforschung - Section A Journal of Physical Sciences*, vol. 23, no. 12, pp. 2135–2136, 1968.

- [47] K. Willets and R. Van Duyne, “Localized surface plasmon resonance spectroscopy and sensing.,” *Annual Review of Physical Chemistry*, vol. 58, pp. 267–297, 2007.
- [48] Y. S. Joe, A. M. Satanin, and C. S. Kim, “Classical analogy of fano resonances.,” *Physica Scripta*, vol. 74, no. 2, pp. 259–266, 2006.
- [49] U. Fano, “Sullo spettro di assorbimento dei gas nobili presso il limite dello spettro d’arco,” *Il Nuovo Cimento (1924-1942)*, vol. 12, no. 3, pp. 154–161, 1935.
- [50] U. Fano, “Effects of configuration interaction on intensities and phase shifts,” *Phys. Rev.*, vol. 124, pp. 1866–1878, 1961.
- [51] H. Beutler, “Über absorptionsserien von argon, krypton und xenon zu termen zwischen den beiden ionisierungsgrenzen.,” *Zeitschrift für Physik A Hadrons and Nuclei*, vol. 93, no. 3-4, p. 177, 1935.
- [52] P. Lambropoulos and D. Petrosyan, *Fundamentals of Quantum Optics and Quantum Information. [electronic resource]*. Berlin, Heidelberg : Springer-Verlag Berlin Heidelberg., 2007.
- [53] A. Taflove and S. C. Hagness, *Computational electrodynamics : The finite-difference time-domain method*. Artech House antennas and propagation library, Boston : Artech House, c2005., 2005.
- [54] A. F. Oskooi, D. Roundy, M. Ibanescu, P. Bermel, J. D. Joannopoulos, and S. G. Johnson, “MEEP: A flexible free-software package for electromagnetic simulations by the FDTD method,” *Computer Physics Communications*, vol. 181, pp. 687–702, 2010.
- [55] J. J. Quinn and K.-S. Yi, *Solid State Physics. [electronic resource] : Principles and Modern Applications*. Berlin, Heidelberg : Springer-Verlag Berlin Heidelberg, 2009., 2009.
- [56] A. D. Rakić, A. B. Djurišić, J. M. Elazar, and M. L. Majewski, “Optical properties of metallic films for vertical-cavity optoelectronic devices,” *Appl. Opt.*, vol. 37, no. 22, pp. 5271–5283, 1998.
- [57] A. Sobhani, A. Manjavacas, Y. Cao, M. J. McClain, F. J. García de Abajo, P. Nordlander, and N. J. Halas, “Pronounced linewidth narrowing of an aluminum nanoparticle plasmon resonance by interaction with an aluminum metallic film,” *Nano Letters*, vol. 15, no. 10, pp. 6946–6951, 2015.
- [58] C. Ayala-Orozco, J. G. Liu, M. W. Knight, Y. Wang, J. K. Day, P. Nordlander, and N. J. Halas, “Fluorescence enhancement of molecules inside a gold nanomatryoshka.,” *Nano Letters*, vol. 14, no. 5, pp. 2926 – 2933, 2014.

- [59] D. V. Voronine, W. Huo, and M. Scully, “Ultrafast dynamics of surface plasmon nanolasers with quantum coherence and external plasmonic feedback.,” *Journal of Optics*, vol. 16, no. 11, p. 114013, 2014.
- [60] K. E. Dorfman, P. K. Jha, D. V. Voronine, P. Genevet, F. Capasso, and M. O. Scully, “Quantum coherence enhanced surface plasmon amplification by stimulated emission of radiation.,” *Phys. Rev. Lett.*, vol. 111, p. 043601, 2013.
- [61] D. V. Voronine, A. M. Sinyukov, X. Hua, E. Munusamy, G. Ariunbold, A. V. Sokolov, and M. O. Scully, “Complex line shapes in surface enhanced coherent raman spectroscopy.,” *Journal of Modern Optics*, vol. 62, no. 2, pp. 90–96, 2015.
- [62] K. Kneipp, Y. Wang, H. Kneipp, L. T. Perelman, I. Itzkan, R. R. Dasari, and M. S. Feld, “Single molecule detection using surface-enhanced raman scattering (sers),” *Phys. Rev. Lett.*, vol. 78, pp. 1667–1670, 1997.
- [63] F. De Angelis, G. Das, P. Candeloro, M. Patrini, M. Galli, A. Bek, M. Lazzarino, I. Maksymov, C. Liberale, L. C. Andreani, and E. Di Fabrizio, “Nanoscale chemical mapping using three-dimensional adiabatic compression of surface plasmon polaritons.,” *Nature Nanotechnology*, vol. 5, no. 1, pp. 67 – 72, 2010.
- [64] C.-H. Hsieh, L.-J. Chou, G.-R. Lin, Y. Bando, and D. Golberg, “Nanophotonic switch: Gold-in-ga2o3 peapod nanowires,” *Nano Letters*, vol. 8, no. 10, pp. 3081–3085, 2008.
- [65] H. A. Atwater and A. Polman, “Plasmonics for improved photovoltaic devices.,” *Nature Materials*, vol. 9, no. 3, pp. 205 – 213, 2010.
- [66] W. Li, A. K. Tuchman, H.-C. Chien, and M. A. Kasevich, “Extended coherence time with atom-number squeezed states,” *Phys. Rev. Lett.*, vol. 98, p. 040402, 2007.
- [67] G.-B. Jo, Y. Shin, S. Will, T. A. Pasquini, M. Saba, W. Ketterle, D. E. Pritchard, M. Vengalattore, and M. Prentiss, “Long phase coherence time and number squeezing of two bose-einstein condensates on an atom chip,” *Phys. Rev. Lett.*, vol. 98, p. 030407, 2007.
- [68] E. Altewischer, M. P. van Exter, and J. P. Woerdman, “Plasmon-assisted transmission of entangled photons.,” *Nature*, no. 6895, p. 304, 2002.
- [69] J. Toulouse, “Optical nonlinearities in fibers: Review, recent examples, and systems applications.,” *Journal of Lightwave Technology*, vol. 23, no. 11, pp. 3625 – 3641, 2005.
- [70] J. Wiersig and M. Hentschel, “Unidirectional light emission from high- q modes in optical microcavities,” *Phys. Rev. A*, vol. 73, p. 031802, 2006.

- [71] U. Hohenester and A. Trugler, “Mnpbem - a matlab toolbox for the simulation of plasmonic nanoparticles.” *Computer Physics Communications*, vol. 183, no. 2, pp. 370–381, 2012.
- [72] N. B. Grosse, J. Heckmann, and U. Woggon, “Nonlinear plasmon-photon interaction resolved by k -space spectroscopy,” *Phys. Rev. Lett.*, vol. 108, p. 136802, 2012.
- [73] S. Coskun, B. Aksoy, and H. E. Unalan, “Polyol synthesis of silver nanowires: An extensive parametric study,” *Crystal Growth and Design*, vol. 11, no. 11, pp. 4963–4969, 2011.
- [74] B. J. Wiley, Y. Xiong, Y. Xia, Z. Y. Li, and Y. Yin, “Right bipyramids of silver: A new shape derived from single twinned seeds,” *Nano Letters*, vol. 6, no. 4, pp. 765–768, 2006.
- [75] J. P. Kottmann, O. J. Martin, D. R. Smith, and S. Schultz, “Plasmon resonances of silver nanowires with a nonregular cross section,” *Physical Review B*, vol. 64, no. 23, p. 235402, 2001.
- [76] J.-J. Zhu, C.-X. Kan, J.-G. Wan, M. Han, and G.-H. Wang, “High-yield synthesis of uniform ag nanowires with high aspect ratios by introducing the long-chain pvp in an improved polyol process,” *Journal of Nanomaterials*, vol. 2011, p. 40, 2011.
- [77] C. Guo, T. Sun, F. Cao, Z. Ren, and Q. Liu, “Metallic nanostructures for light trapping in energy-harvesting devices,” *Light: Science and Applications*, vol. 3, 2014.
- [78] B. C. Yildiz, M. E. Tasgin, M. K. Abak, S. Coskun, H. E. Unalan, and A. Bek, “Enhanced second harmonic generation from coupled asymmetric plasmonic metal nanostructures,” *Journal of Optics*, vol. 17, no. 12, p. 125005, 2015.

CURRICULUM VITAE

PERSONAL INFORMATION

Surname, Name: Yıldız Karakul, Bilge Can

Nationality: Turkish (TC)

Date and Place of Birth: 08.11.1984, Ankara

Marital Status: Married with one child (2015)

Phone: 0 505 4481245

Fax: 0 312 2105099

EDUCATION

Degree	Institution	Year of Graduation
M.S.	Department of Physics, METU	2011
B.S.	Department of Physics, METU	2009
High School	Fethiye Kemal Mumcu Anadolu Lisesi	2002

PROFESSIONAL EXPERIENCE

Year	Place	Enrollment
2011-Present	Department of Applied Physics, Atılım University	Research Assistant

PUBLICATIONS

Proceedings Presented in National/International Meetings

1. B. C. Yildiz, M. E. Tasgin, M. K. Abak, and A. Bek, Enhanced second harmonic generation from coupled asymmetric plasmonic metal nanostructures, European Conference on Surface Science (ECOSS-30), August 31 – September 5 2014 Antalya, Turkey (oral presentation)
2. B. C. Yildiz, M. E. Tasgin, M. K. Abak, S. Coskun, H. E. Unalan, and A. Bek, Enhanced second harmonic generation from coupled asymmetric plasmonic metal nanostructures, SolarTR-3 Third Turkish Solar Electricity Conference and Exhibition, April 27-29 2015 Ankara, Turkey (poster presentation)
3. B. C. Yildiz, M. E. Tasgin, H. E. Unalan, and A. Bek, All-plasmonic enhancement of second harmonic generation via interference of conversion paths, COST Action MP1403 Nanoscale Quantum Optics WG2-WG3 Workshop, May 30 – June 2 2016 Marseille, France (oral presentation)
4. B. C. Yildiz, M. E. Tasgin, H. E. Unalan, and A. Bek, Enhancing second harmonic conversion of plasmonic systems via Fano-coupling mechanism, 8th Mediterranean Conference on Nano-Photonics (MEDINANO 2016), June 29-30 2016 Athens, Greece (oral presentation)
5. B. C. Yildiz, A. Bek, Nonlinear conversion of continuous wave light by molecular-plasmonic and all-plasmonic hybrid nanostructures, Science and Applications of Thin Films Conference and Exhibition (SATF 2016), September 19-23, 2016, İzmir, Turkey (oral presentation)

International Journal Publications

1. B. C. Yildiz, M. E. Tasgin, M. K. Abak, S. Coskun, H. E. Unalan, and A. Bek, “Enhanced second harmonic generation from coupled asymmetric plasmonic metal nanostructures,” *Journal of Optics*, vol. 17, no. 12, p. 125005, 2015.